

## Article

# Innovative Methylcellulose-Polyvinyl Pyrrolidone-Based Solid Polymer Electrolytes Impregnated with Potassium Salt: Ion Conduction and Thermal Properties

Abdullahi Abbas Adam <sup>1,2,3,\*</sup>, Mohammed Khalil Mohammed Ali <sup>4,\*</sup>, John Ojur Dennis <sup>1</sup>, Hassan Soleimani <sup>1</sup>, Muhammad Fadhullullah Bin Abd. Shukur <sup>1,2</sup>, Khalid Hassan Ibnaouf <sup>4</sup>, Osamah A. Aldaghri <sup>4</sup>, Moez A. Ibrahim <sup>4</sup>, Naglaa F. M. Abdel All <sup>4</sup> and Abubakar Bashir Abdulkadir <sup>1,2</sup>

<sup>1</sup> Department of Fundamental and Applied Sciences, Universiti Teknologi PETRONAS, Seri Iskandar 32610, Malaysia; jdennis100@gmail.com (J.O.D.); hassan.soleimani@utp.edu.my (H.S.); mfadhullullah.ashukur@utp.edu.my (M.F.B.A.S.); abubakarbashir150@gmail.com (A.B.A.)

<sup>2</sup> Centre of Innovative Nanoscience and Nanotechnology (COINN), Universiti Teknologi PETRONAS, Seri Iskandar 32610, Malaysia

<sup>3</sup> Department of Physics, Al-Qalam University Katsina, Katsina 820252, Nigeria

<sup>4</sup> Department of Physics, College of Science, Imam Mohammad Ibn Saud Islamic University (IMSIU), Riyadh 13318, Saudi Arabia; khiahmed@imamu.edu.sa (K.H.I.); odaghri@imamu.edu.sa (O.A.A.); 9@imamm.org (M.A.I.); nfabdelall@imamu.edu.sa (N.F.M.A.A.)

\* Correspondence: abbasabdullah17@hotmail.com (A.A.A.); mkali@imamu.edu.sa (M.K.M.A.)



**Citation:** Adam, A.A.; Ali, M.K.M.; Dennis, J.O.; Soleimani, H.; Shukur, M.F.B.A.; Ibnaouf, K.H.; Aldaghri, O.A.; Ibrahim, M.A.; Abdel All, N.F.M.; Bashir Abdulkadir, A. Innovative Methylcellulose-Polyvinyl Pyrrolidone-Based Solid Polymer Electrolytes Impregnated with Potassium Salt: Ion Conduction and Thermal Properties. *Polymers* **2022**, *14*, 3055. <https://doi.org/10.3390/polym14153055>

Academic Editor: Luis Alves

Received: 26 June 2022

Accepted: 25 July 2022

Published: 28 July 2022

**Publisher's Note:** MDPI stays neutral with regard to jurisdictional claims in published maps and institutional affiliations.



**Copyright:** © 2022 by the authors. Licensee MDPI, Basel, Switzerland. This article is an open access article distributed under the terms and conditions of the Creative Commons Attribution (CC BY) license (<https://creativecommons.org/licenses/by/4.0/>).

**Abstract:** In this research, innovative green and sustainable solid polymer electrolytes (SPEs) based on plasticized methylcellulose/polyvinyl pyrrolidone/potassium carbonate (MC/PVP/K<sub>2</sub>CO<sub>3</sub>) were examined. The MC/PVP/K<sub>2</sub>CO<sub>3</sub> SPE system with five distinct ethylene carbonate (EC) concentrations as a plasticizer was successfully designed. Frequency-dependent conductivity plots were used to investigate the conduction mechanism of the SPEs. Electrochemical potential window stability and the cation transfer number of the SPEs were studied via linear sweep voltammetry (LSV) and transference number measurement (TNM), respectively. Additionally, the structural behavior of the SPEs was analyzed using Fourier transform infrared spectroscopy (FTIR), field emission scanning electron microscopy (FESEM), X-ray diffractometry (XRD), and differential scanning calorimetry (DSC) techniques. The SPE film complexed with 15 wt.% EC measured a maximum conductivity of  $3.88 \times 10^{-4} \text{ Scm}^{-1}$ . According to the results of the transference number examination, cations that record a transference number of 0.949 are the primary charge carriers. An EDLC was fabricated based on the highest conducting sample that recorded a specific capacitance of 54.936 Fg<sup>-1</sup> at 5 mVs<sup>-1</sup>.

**Keywords:** methylcellulose; polyvinyl pyrrolidone; potassium carbonate; ethylene carbonate; solid polymer electrolytes

## 1. Introduction

Recently, solid-state electrolytes (SSEs) have arisen as a technology of significant research and commercial relevance for the storage of electrical energy. Solid polymer electrolytes (SPEs) are a class of SSEs that comprise an inorganic salt dispersed in a polymer host material [1]. Currently, SPEs are getting particular attention due to a variety of factors, including the development of high-performance materials, better safety concerns, and innovative applications [2–5]. By modifying their chemistry, several SPEs now achieve ionic conductivity equivalent to those of liquid electrolytes at room temperature. Additional advantages of SPEs over the liquid type include mechanical stability, excellent film formation with superior ionic conductivity, and self-standing ability [6–14].

To meet the continued demand for low-cost, high-performing, and high-safety electrolyte materials, there is an increasing demand to come up with novel materials for PEs or modify the current ones. Among these materials, special attention is given to SPEs due to

their fascinating properties. In comparison to liquid and gel electrolytes, SPEs have several advantageous characteristics, including a lack of leakage; excellent thermal, electrochemical, and volumetric stabilities; absence of solvents; and low volatility. Other properties that are attracting increased interest in SPEs include high potential stability, superior mechanical strength, longer cycle life, simple processing and fabrication, lightweight, high automation process, high energy density, flexibility, and the ability to be configured in a number of different geometries [15].

Cellulose (the most abundant natural biopolymer) and its derivatives are widely used in SPEs, primarily for their biodegradability, low cost, and environmental friendliness [4,16]. Among the cellulose derivatives, methylcellulose (MC) is a distinctively water-soluble semicrystalline polymer with an ionic conductivity of around  $10^{-11} \text{ Scm}^{-1}$  [17,18]. However, this magnitude is insufficient for practical use in SPEs' technology. By modifying the chemistry of MC, it has shown promising ionic conductivity in the amorphous phase, allowing for better ion transport inside the polymer [6,19]. According to previous reports [20,21], blending polymers improves the electrochemical and physicochemical properties of the electrolyte system by expediting the ion migration process and providing additional complexation sites within the polymer matrix. Specifically, blending MC with another polymer has been an effective way to augment the amorphous nature of MC-based SPEs [22–24].

In addition to natural-based polymers such as MC, there has also been an extensive investigation on SPEs based on synthetic polymers such as polyvinyl alcohol (PVA) [25–27], polyvinylidene fluoride (PVDF) [28,29], polyethylene oxide (PEO) [30,31], and polyvinyl pyrrolidone (PVP) [32–35]. Among these polymers, PVP has recently received much interest due to its amorphous structure, biocompatibility, high glass transition temperature, high solubility in water, and the potential to form complexes with various salts [32–36]. The PVP pyrrolidine groups are responsible for good ionic mobility while the carbonyl groups are responsible for the formation of various complexes with different salts [37]. Therefore, mixing PVP with other synthetic or natural polymers will expectedly result in a plasticized polymer blending with high amorphousness and increased ion mobility in the amorphous phase.

Due to their rapid cation mobility and strong ionic conductivity, potassium salts have shown their suitability for use in SPEs, among alkali metal salts. Because potassium is a big cation, it is seldom entrapped by polymeric networks; hence,  $\text{K}^+$  movement within the polymer matrix requires less activation energy [38]. In this study,  $\text{K}_2\text{CO}_3$  was chosen as a conducting salt due to its strong propensity to dissociate because of its large ion size and high ionic conductivity-free ions. In addition to its high ion content, superior thermal stability, non-volatility, non-combustibility, low viscosity, and environmental friendliness, it also has a low viscosity [39,40]. Furthermore,  $\text{K}_2\text{CO}_3$  was selected owing to its high plasticizing action, hydrophilic characteristics, and inexpensive cost. The  $\text{K}^+$  from  $\text{K}_2\text{CO}_3$  is a cation with a tiny radius; thus, tiny cations may be readily dissociated and transferred as charge carriers or ions in SPEs [41].

The solution casting procedure is a well-known technique for preparing stand-alone films and is less complicated compared to other methods such as electrochemical deposition [42], sol-gel [43], and citrate-gel combustion [44]. To obtain SPE with great mechanical, thermal, and electrical qualities, it is critical to choose polymers that are compatible with one another and with the salt [45]. Thus, in this work, we report the synthesis of a new SPE based on an MC and PVP blend doped with potassium carbonate ( $\text{K}_2\text{CO}_3$ ) using the conventional solution casting technique. The concentration of  $\text{K}_2\text{CO}_3$  was varied to investigate the effect of  $\text{K}^+$  in the solid electrolyte films. To further improve the conductivity of the prepared samples, the highest conducting sample was plasticized with EC at various concentrations, and the effects of EC on conductivity, potential stability, and crystallinity were studied.

## 2. Materials and Methods

### 2.1. Materials

MC (viscosity of 4000 cP) and PVP ( $M_w$  of 40,000  $\text{g mol}^{-1}$ ) were procured from Sigma Aldrich, Malaysia, through Evergreen Chemicals Supply (Selangor Malaysia).  $\text{K}_2\text{CO}_3$  ( $M_w$  of 138.21  $\text{g mol}^{-1}$ ) and EC ( $M_w$  of 88.06  $\text{g mol}^{-1}$ ) were purchased from R and M Chemicals. All chemicals were used as supplied without any treatment. DI water was used as the only solvent throughout the experiment.

#### 2.1.1. Synthesis of MC/PVP Polymer Blend

A required mass of MC (1.0–0.5 g) was dissolved in DI water (100 mL) and stirred at 50 °C for a few hours until fully dissolved. The PVP (0–0.5 g) was added to the MC solution and stirred at room temperature for a few hours to obtain a homogenous solution. To ensure total and homogenous blending, the solution was then sonicated for 1 h followed by 30 min of additional stirring at room temperature. Using this approach, six different samples containing different ratios of MC to PVP (100:0, 90:10, 80:20, 70:30, 60:40, and 50:50) were prepared. Samples containing higher concentrations of PVP were not prepared because stand-alone films could not be synthesized due to their extremely poor mechanical strength. Each solution was cast on a petri dish and covered with a filter paper (to avoid contamination) to dry at room temperature for 3 to 5 days. Prepared films were stored in a desiccator. To easily identify the prepared samples, they were labeled MP0, MP10, MP20, MP30, MP40, and MP50 for the various concentrations of PVP in the samples. A typical image of a prepared MC/PVP SPE film is shown in Figure 1. It is worth stating that a stand-alone film was not obtained when the concentration of PVP was higher than that of MC. Rather, the film stuck firmly to the petri dish, as can be seen in Figure S1. Furthermore, the prepared SPEs were extremely flexible and durable against different forms of manipulations, as can be seen in Figure S2.

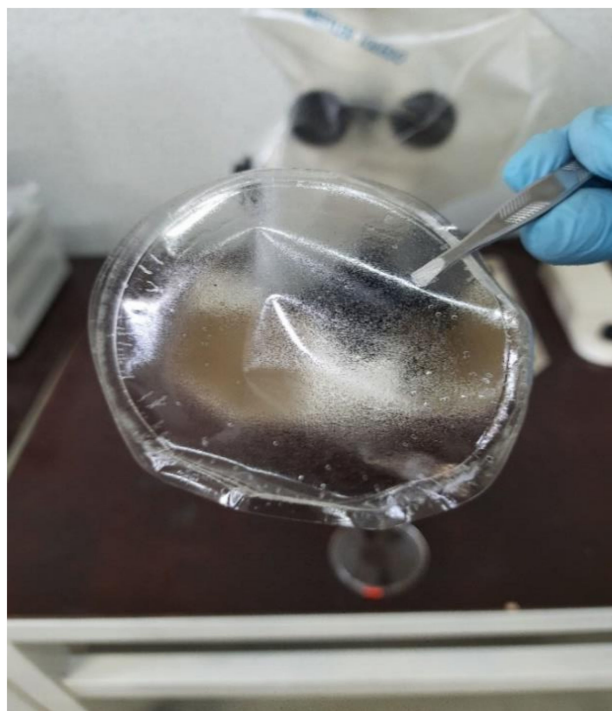


**Figure 1.** MC/PVP SPE film.

#### 2.1.2. Synthesis of MC/PVP/ $\text{K}_2\text{CO}_3$ SPE

To the most amorphous MC/PVP electrolyte (MP50),  $\text{K}_2\text{CO}_3$  was added to prepare the MC/PVP/ $\text{K}_2\text{CO}_3$  SPE films in a similar way to that in which MC/PVP was prepared. In brief, MC (0.5 g) was dissolved in 100 mL of DI water under stirring at 50 °C. When it

was fully dissolved, an equal mass of PVP was added and the mixed solution was stirred at room temperature until a homogenous solution was obtained. Next, 5–25 wt.% of  $K_2CO_3$  was added to five different MC/PVP solutions and each solution was stirred for 1 h. The solutions were then sonicated for 1 h followed by stirring on a hot plate for 30 min (at room temperature) to ensure the complete dispersion of  $K_2CO_3$ . Each solution was then poured onto a petri dish, covered with filter paper, and stored at room temperature to dry gradually. To ensure nearly equal film thickness, the volumes of all electrolyte samples cast on petri dishes were maintained at 40 mL. Dried films were peeled off and stored in a desiccator for further drying before characterization. Prepared samples containing different concentrations of potassium salt were labeled as MPK5, MPK10, MPK15, MPK20, and MPK25. The flow diagram depicting the synthesis of the prepared SPE is presented in Figure 2.

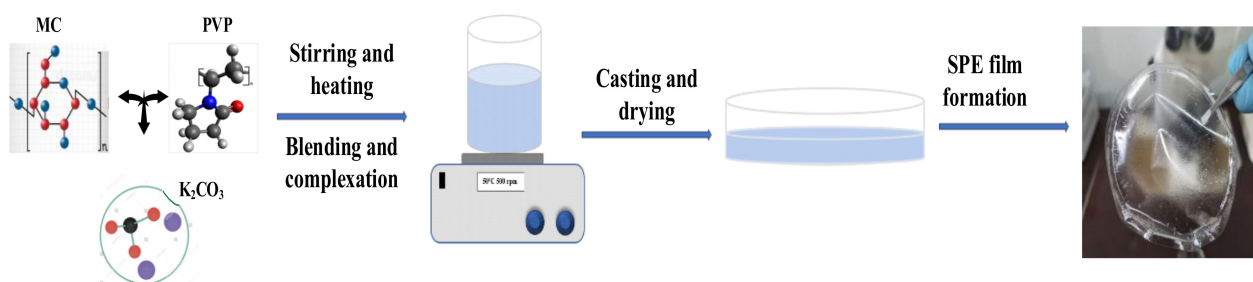


**Figure 2.** Flow diagram showing the preparation of MC/PVP/ $K_2CO_3$  SPEs.

### 2.1.3. Synthesis of MC/PVP/ $K_2CO_3$ /EC SPE

To prepare plasticized samples, EC was incorporated into MPK20, which was the SPE with the highest ionic conductivity. The salted samples were prepared according to the explanation in Section 2.1.2 above. When the polymer-salt complex solution is fully dissolved, 5–25 wt.% (interval of 5) EC plasticizer was added to the solution and stirred for 20 min before sonication for another 20 min. Finally, the solution was further stirred for 30 min (at room temp) and allowed to settle for 1 h to expel air bubbles before casting. Each solution was cast on petri dish and dried at room temperature. Dried films were peeled off and stored in a desiccator for further drying before characterization. To denote the samples containing different amounts of EC, the following codes were used: MPKE5, MPKE10, MPKE15, MPKE20, and MPKE25.

### 2.1.4. EDLC Fabrication

The supercapacitor (EDLC) was fabricated by sandwiching the most conductive electrolyte (MPKE15) between two activated carbon (AC) electrodes produced and packed inside a CR2032 coin cell. To begin the preparation of the electrode, 1 g of polyvinylidene fluoride (PVdF) was dissolved in 30 mL of N-methyl pyrrolidone (NMP) and stirred at 50 °C. After 20 min, the solution was cooled to room temperature while being constantly stirred. Meanwhile, 0.5 g of carbon black (acetylene black) was added and mixed for 2 h at room temperature. Finally, 6.5 g of AC was added gradually, and the mixture was stirred until it was completely dissolved. The slurry was ultrasonically treated for 30 min (to guarantee homogeneity) followed by further stirring on a hot plate at room temperature for a further 1 h and then cooled to room temperature. The produced slurry was coated on nickel foams that were previously pressed and weighed. The coated nickel foams were dried at 50 °C for 24 h and then re-weighed to calculate the mass of the deposited slurry. AC electrodes of equivalent slurry mass were matched for the production of the EDLC.

## 2.2. Characterization of Electrolyte Samples

Fourier transform infrared (FTIR) studies of the prepared films were conducted on an FTIR spectrometer (Bruker Instruments, model Aquinox 55, Germany) in the 4000–400  $cm^{-1}$  range using KBr pellets with a scanning resolution of 4  $cm^{-1}$ . To analyze the crystal struc-

ture for prepared films, X-ray diffraction (XRD) was carried out using a 40 kV Bruker D8 Advance X-ray diffractometer with a current of 40 mA using a Ni-filtered Cu K $\alpha$  graphite monochromator ( $\lambda = 1.5406 \text{ \AA}$ ). The study of surface morphology of the synthesized samples was examined using field emission scanning electron microscopy (FESEM) [46,47]. Differential scanning calorimetry (DSC) (model DSC Q2000 V24.11, Oberkochen, Germany) was used to investigate the thermal behavior of the SPEs. The glass transition temperature ( $T_g$ ) of the samples was measured at a heating rate of  $10 \text{ }^\circ\text{Cm}^{-1}$  from  $-50 \text{ }^\circ\text{C}$  to  $190 \text{ }^\circ\text{C}$  in a nitrogen ( $\text{N}_2$ ) environment.

### 2.3. Electrochemical Studies of Solid Electrolytes

The electrochemical studies were performed to analyze the ionic conductivity and operating potential window of each polymer electrolyte. The measurement was performed in the two electrodes' system using AUTOLAB/AUT51018. The SPE sample was sandwiched between two blocks of a stainless-steel sample holder with a  $3.142 \text{ cm}^2$  surface area that were positioned opposite each other. Transference number measurement (TNM) was performed using a digital DC power supply (V&A Instrument DP3003).

### 2.4. EDLC Characterization

#### Cyclic Voltammetry (CV)

The electrochemical characteristics of EDLC were investigated using eight different scan rates:  $5 \text{ mVs}^{-1}$ ,  $10 \text{ mVs}^{-1}$ ,  $20 \text{ mVs}^{-1}$ ,  $40 \text{ mVs}^{-1}$ ,  $80 \text{ mVs}^{-1}$ ,  $100 \text{ mVs}^{-1}$ ,  $200 \text{ mVs}^{-1}$ , and  $500 \text{ mVs}^{-1}$  in the potential range between  $-0.9 \text{ V}$  and  $0.9 \text{ V}$ . To characterize the EDLC, a potentiostat (AUTOLAB/AUT51018) equipped with Nova 2.1.4 software was employed. Using the following formula [3], the specific capacitance ( $C_{sp}$ ) of EDLC cells was determined.

$$C_{sp} = \frac{1}{2mv(V_f - V_i)} \int_{V_i}^{V_f} I(V)dV \quad (1)$$

where  $I(V)dV$  represents the CV's area as calculated by the OriginPro 2021's program integration function. The parameters  $m$  and  $v$  are the average mass of active materials and scan rate, respectively. In this study, the initial and final applied potentials ( $V_i$  and  $V_f$ ) were  $-0.9 \text{ V}$  and  $0.9 \text{ V}$ , respectively.

## 3. Results and Discussion

### 3.1. Structural Analysis

#### 3.1.1. FTIR Studies

"FTIR is a direct method to distinguish molecular interactions by monitoring the band shifts of certain functional groups" [48]. The FTIR spectra of the MC/PVP polymer blend within the range of  $800\text{--}4000 \text{ cm}^{-1}$  are presented in Figure 3 and the band assignments are shown in Table 1. For pure MC, absorption peaks were observed at  $3479 \text{ cm}^{-1}$ ,  $2907 \text{ cm}^{-1}$ , and  $1057 \text{ cm}^{-1}$ , which correspond to O-H stretching, C-H (in  $\text{CH}_2$ ) stretching, and C-O-C stretching, respectively [7,21,46]. Similarly, pure PVP exhibited distinctive peaks at  $2918 \text{ cm}^{-1}$ ,  $1614 \text{ cm}^{-1}$ , and around  $1500 \text{ cm}^{-1}$ , which were attributed to C-H stretching, C=O stretching, and C-N stretching, respectively [32,47,48]. As reported by Hamsan et al. [16], the interaction between two polymers in a blend system is indicated by the shifting of the FTIR peaks of the functional groups containing oxygen atoms (such as hydroxyl and ether groups). Thus, we investigated the blending of MC with PVP by observing the band shift in the polymer blend systems.

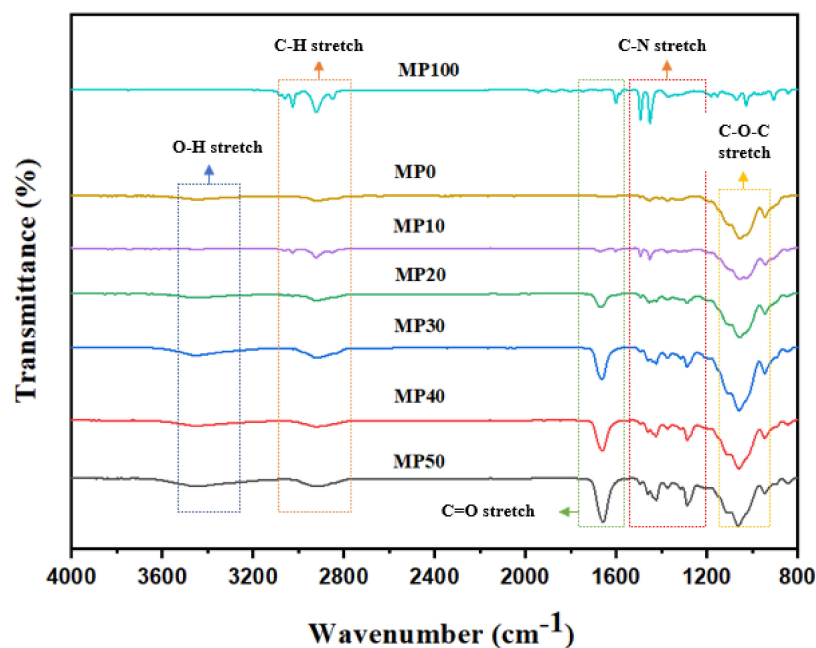


Figure 3. FTIR of MC/PVP polymer blend.

When MC blends with another polymer, the shift in the FTIR peaks occur at the oxygen atom-containing functional groups of MC [21]. In the MC/PVP polymer blend, the hydrogen atoms in PVP form hydrogen bonds with the oxygen atoms of the hydroxyl groups of MC (or vice versa). Here, we may assume that the oxygen atoms in MC's O–H groups formed short-ranged hydrogen bonds with the corresponding hydrogen atoms of PVP. For MP10, the O–H stretch shifted to  $3436\text{ cm}^{-1}$  due to the hydrogen bond interaction between the two polymers. As the concentration of PVP increased, the O–H band of the polymer blend shifted further to a higher wavelength region (as shown in Table S1). These results clearly indicated that MC and PVP blended homogeneously, and the amorphous structure of the polymer blend increased with increasing PVP concentration, as confirmed by XRD patterns.

It was evidently clear that a complex system was formed when salt and the polymer matrix interacted. The presence of complete complexation between salt cations and polymer functional groups is indicated by a decrease in transmittance intensity and a change in band position [6]. As a result of the electrostatic synergy between the functional group and the salt cation, the vibration inside the polar group was diminished. Changes in peak location imply principally the change in the state of the electron dispersion or hybridization inside the chemical bond. Typically, a reduction in peak intensity indicates a decrease in the number of functional groups linked with the molecular bond (per unit volume) [49,50].

Here, when MP50 was doped with varying amounts of  $\text{K}_2\text{CO}_3$  (Figure 4), the OH stretch not only broadened, it equally downshifted, indicating the development of a polymer-salt complex [21,51,52]. The shift in the OH band spectrum was attributed to the reciprocating between the  $\text{K}^+$  hopping mechanism and MC/PVP host segmental motion. The potassium atom in  $\text{K}_2\text{CO}_3$  readily dissociated from the parent molecule to create  $\text{K}^+$  and wandered within the polymer matrix. As a result of its free movement within the polymer structure, the  $\text{K}^+$  facilitated conduction inside the polymer matrix. The anticipated polymer-salt complexation for the prepared SPE is shown in Figure 5. According to Hamsan et al. [47], an increase in salt content increases the number of cations that may interact with the oxygen atom of the hydroxyl or carbonyl groups of MC/PVP, leading to an increase in ionic conductivity. However, the IR spectrum corresponding to the OH stretch nearly disappeared for MPK25. This denoted the formation of neutral ion pairs via ion recombination. The production of neutral ion pairs may decrease the quantity of charge carriers in a polymer matrix, hence lowering its ionic conductivity [47].

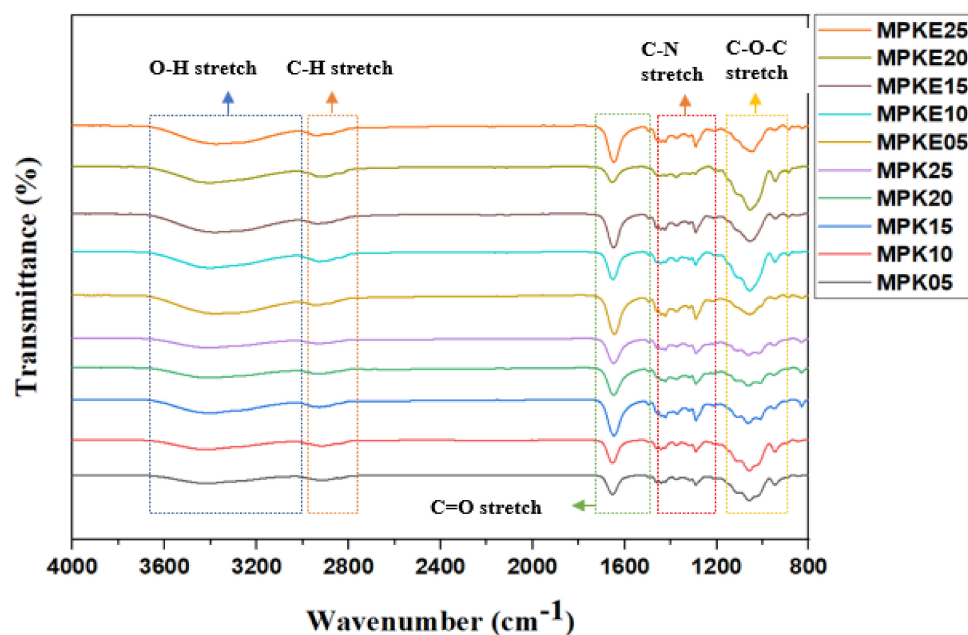


Figure 4. FTIR of plasticized and non-plasticized MC/PVP/K<sub>2</sub>CO<sub>3</sub> SPEs.

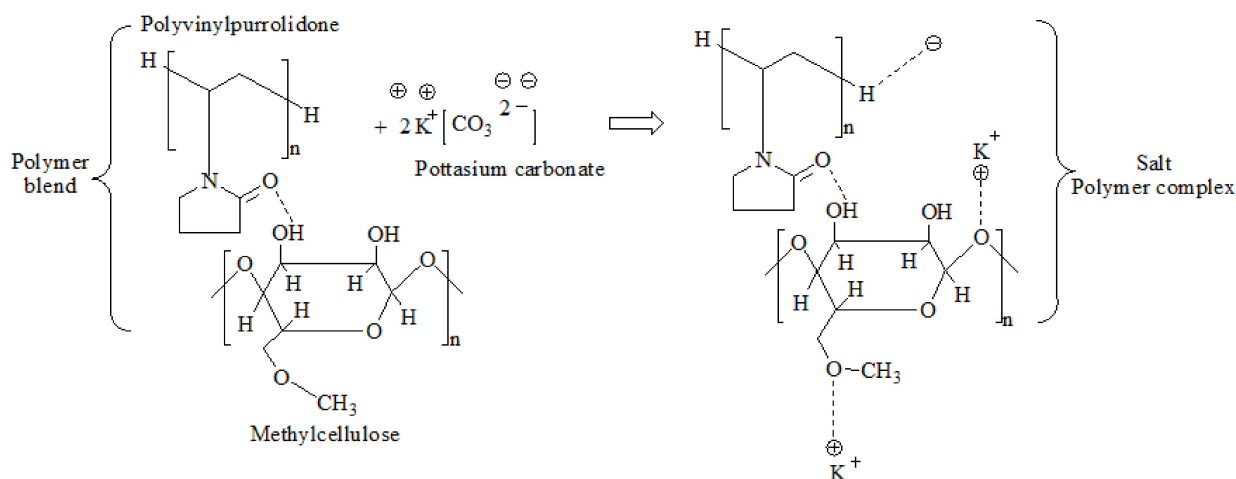


Figure 5. Schematic representation of MC/PVP/K<sub>2</sub>CO<sub>3</sub> polymer-salt complexation.

On a closer look, the FTIR spectra of the EC plasticized samples demonstrated that the spectrum of each MPKE film was almost identical to that of MPK50. However, the intensities of certain peaks (OH and COC) varied appreciably. C=O in the EC may have interacted with the alkyl group of MC/PVP molecular chains, which might have contributed to the band shift observed at the OH and COC regions. A potential reason is that EC may have interacted with K<sub>2</sub>CO<sub>3</sub>, hence altering K<sub>2</sub>CO<sub>3</sub>'s interaction with the MC/PVP skeleton. Generally, ion dissociation is facilitated when a plasticizer is added to the polymer-salt complex. This enables additional ions to interact with the polymer's functional groups [48]. The increase in EC concentration causes a change in the transmittance intensity due to ion-dipole complexation resulting from an increased number of K<sup>+</sup>. Increasing EC content increases K<sub>2</sub>CO<sub>3</sub> dissolution. The increased coordination between K<sup>+</sup> and the C=O segment of EC results in enhanced dissociation of K<sup>+</sup>, thereby generating a weak bond that promotes electron conduction via the delocalized pi system [53,54]. In addition, these weak bonds provide alternative routes for K<sup>+</sup> to enter the coordinating sites of the MC/PVP backbone.

Plasticizers are believed to play a role as spacers between polymer molecules by creating linkages with them as a result of dipole couplings between polar groups in the plasticizer [48,55]. As a result of the presence of EC, the Coulombic force between K<sub>2</sub>CO<sub>3</sub>

cations and anions was lowered. Consequently, more salts were dissociated into free mobile ions, increasing the ion density and the conductivity [56,57]. However, the addition of more than 15 wt.% EC reduces the conductivity of the SPE. This is due to the displacement of  $K_2CO_3$  inside the polymer-salt complexes by EC molecules, which cause the salt to recrystallize, resulting in a decrease in conductivity.

### 3.1.2. XRD Analysis

An XRD study was employed to investigate the crystallinity of MC/PVP SPE films and to analyze the formation of the MC/PVP blend system [58]. The structure and phase patterns of MC/PVP SPEs are presented in Figure 6. According to the literature [59,60], MC has a prominent broad peak around  $19\text{--}22^\circ$ , which is a characteristic of its semicrystalline structure resulting from hydrogen bonding at both the intermolecular and intramolecular levels. In most cases, a relatively sharp peak can also be observed in the MC film at  $8^\circ$ . This peak is attributed to a sequence of trimethyl cellulose present in MC [59]. Because PVP (MP100) is completely amorphous, crystalline peaks are barely observed. However, two broad amorphous bands are usually noticed around  $2\theta = 11^\circ$  and  $22^\circ$  [61]. From the XRD patterns obtained in this study, MC peaks were observed at  $2\theta = 7.8^\circ$  and  $20.2^\circ$  while amorphous PVP exhibited two hollows at  $2\theta = 10.9^\circ$  and  $19.6^\circ$ . This result is consistent with some of the reported literature [7,61,62]. The XRD pattern showed a steady decline in the intensity of the MC peak upon the addition of varying concentrations of PVP. Similarly, the hollows observed in PVP equally disappeared as the MC/PVP composite was being formed. The increase in the amorphous phase of the system confirmed the successful blending of MC with PVP. With a further increase in the amount of PVP in the MC precursor, the intensity became more obvious until an optimum result was obtained for the MP50 sample. Thus, MP50 was taken as the optimum sample for further studies.

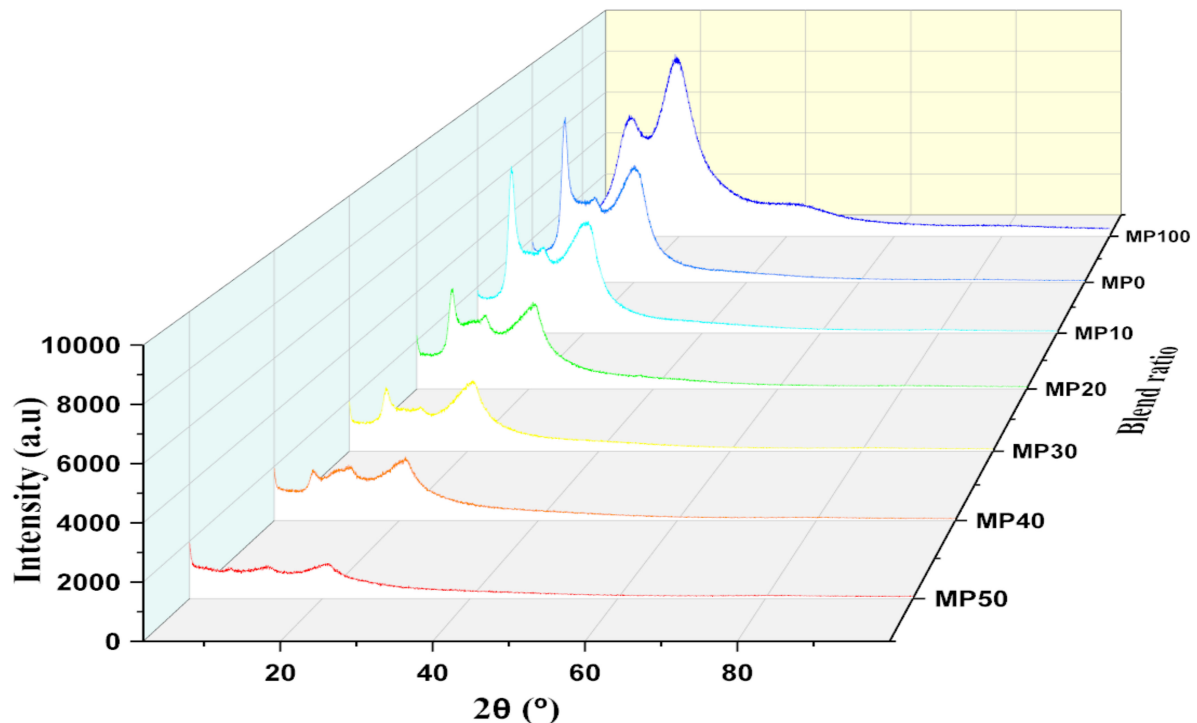


Figure 6. XRD pattern of the MC/PVP polymer blend.

### 3.2. Morphological Analysis

#### FESEM Analysis

FESEM micrographs can provide an understanding of the compatibility of the various components of a composite SPE and their interfaces. In addition, the surface examination

enables one to understand the alterations in the structural and electrical characteristics of SPEs [52]. According to Hamsan et al. [24], a cross-sectional view of an FESEM micrograph is an excellent way to study the miscibility of polymer blend systems. Figure 7 shows cross-sectional FESEM images of MC/PVP polymer blend systems with the top view shown as an inset. As the micrographs demonstrate, the pure MC (MP0) film exhibited a homogenous, smooth surface, which is a characteristic property of semicrystalline MC. For various MC/PVP blend systems (MP10–MP50), smoother and denser cross-sectional images were obtained due to the incorporation of PVP. The polymer blend system's smoothness was seen to increase as the concentration of PVP increased, mainly due to the amorphous nature of PVP. All FESEM images showed no evidence of phase separation, which showed that MC and PVP were homogeneously blended. Moreover, smoother FESEM images indicate better blending between the polymers and improved amorphous phase. Since the improved amorphous section provided better ion transfer pathways, MP50 seemed to show better morphology compared to other films. This observation was consistent with the XRD and FTIR results previously explained. Similar patterns of increasing amorphousness at higher contents of PVP were seen in the surface view of the FESEM images (shown in insets). Because pure PVP cannot be peeled off from a petri dish, the FESEM of the MP100 film analyzed on a petri dish substrate is shown in Figure S1b. The numerous holes seen on the surface of the film were due to trapped air as the PVP stuck to the substrate, thus forming bubbles.

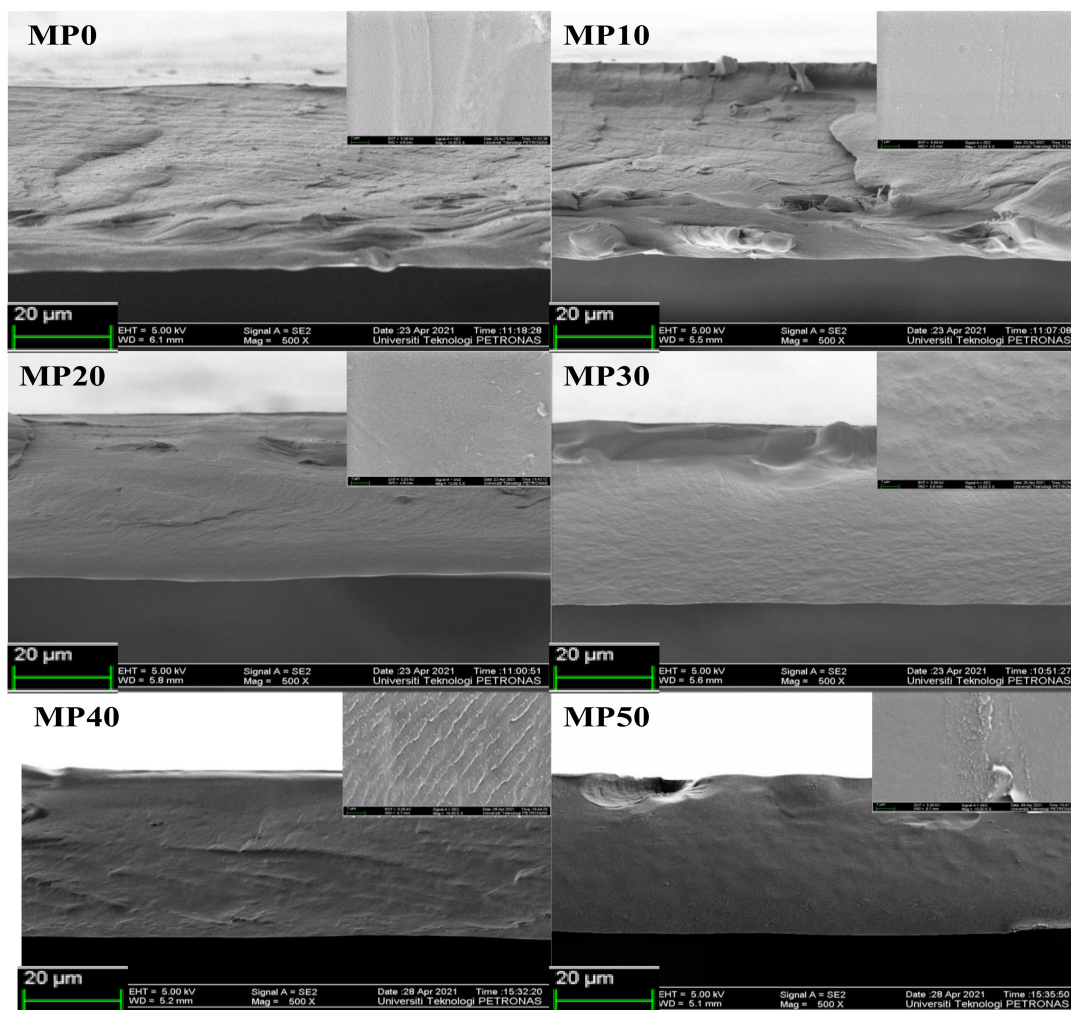


Figure 7. FESEM micrographs of MC/PVP polymer blend.

### 3.3. DSC Analysis

According to Genier et al. [63], the low ionic conductivity of SPEs is caused by the high glass transition temperature and high polymer crystallinity of the host polymers. The thermal behavior of MP50, MPK20, and MPKE15 was examined by DSC analysis. Figure 8 illustrates the alterations in  $T_g$  for the analyzed samples' record between 41–150 °C. All DSC thermograms depicted an endothermic peak with a single step transition, which means that MC and PVP are miscible with each other [21]. The  $T_g$  of MP50 was recorded at 83.69 °C. Upon doping with 20 wt.%  $K_2CO_3$ , the  $T_g$  was lowered to 77.51 °C. The decrease in the  $T_g$  value suggested that the polymer salts' segment became softer in the amorphous phase structure [64], hence improving the segmental mobility of the polymer-salt complex. Moreover, the reduction in  $T_g$  of the polymer host was similarly associated with the increase in ionic conductivity of SPEs. The introduction of the salt into the MC/PVP system weakened the dipole-dipole interactions between the MC/PVP chains. In turn, this allowed the ions to travel freely across the polymer chain network when an electric field was applied, hence enhancing the conductivity [65,66].

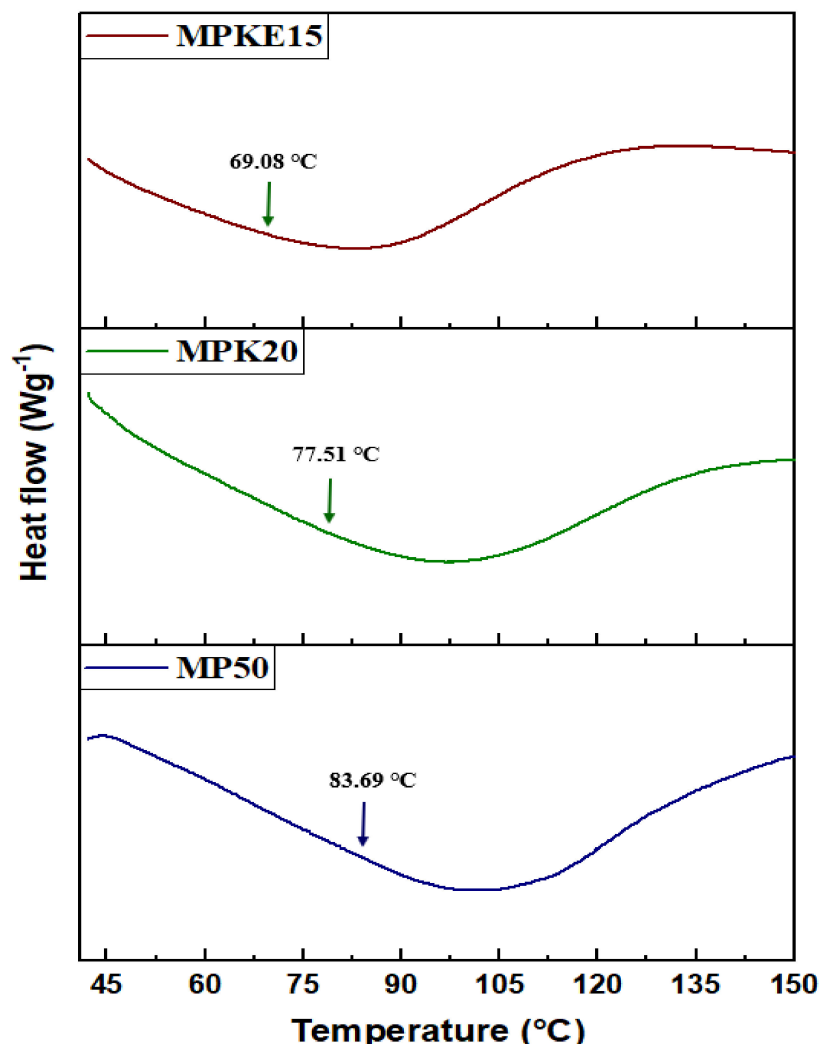


Figure 8. DSC thermograms of selected MC/PVP-based SPEs.

EC was selected for this study because of its high dielectric constant and low vapor pressure. With the addition of EC, it was envisaged that many charge carriers would localize along with the mobile ions, thereby improving the SPE's ionic conductivity [67]. As expected, the DSC thermogram of MPK15 showed a significant decrease in the  $T_g$  value (9.08 °C). This is because the inclusion of EC aided in boosting the amorphous fraction of

SPEs as well as improving the polymer segmental mobility. Feng et al. [68] also reported a similar pattern where they observed that both LiClO<sub>4</sub> and EC cause a shifting of an endothermic peak of the PEO-based SPE to a lower temperature.

### 3.4. Electrochemical Studies

#### 3.4.1. EIS Studies

As stated earlier, AUTOLAB/AUT51018 (potentiostat/galvanostat) was used to study the ionic conductivity of the polymer blend electrolytes over a range of frequencies from 10<sup>-2</sup> Hz to 10<sup>5</sup> Hz and at room temperatures [48]. The Nyquist plots of selected samples (MP50, MPK20, and MPKE15) together with their corresponding electrical circuit model (EEC) are shown in Figure 9. The EEC approach was employed to examine the EIS because it is straightforward and provides a complete view of the system [69]. As seen in the inset, the impedance diagrams are represented by an equivalent circuit composed of a charge transfer resistance ( $R_b$ ) in a parallel configuration with the first constant phase element (CPE1) in the high-frequency area and in a series arrangement with the second constant phase element (CPE2) in the low-frequency region. According to Nofal et al. [38], the impedance due to the CPE ( $Z_{CPE}$ ) can be expressed in terms of the CPE capacitance ( $C$ ) and angular frequency ( $\omega$ ) using Equation (3).

$$Z_{CPE} = \frac{1}{C\omega^\rho} \left[ \cos\left(\frac{\pi\rho}{2}\right) - i\sin\left(\frac{\pi\rho}{2}\right) \right] \quad (2)$$

In the above equation,  $\rho$  defines the EIS deviation from the imaginary axis. The real and imaginary impedance ( $Z_r$  and  $Z_i$ ) associated with the EEC are given as:

$$Z_r = \frac{R_b^2 C_1 \omega^{\rho_1} \cos(\pi\rho_1/2) + R_b}{2R_b C_1 \omega^{\rho_1} \cos(\pi\rho_1/2) + R_b^2 C_1^2 \omega^{2\rho_1} + 1} + \frac{\cos(\pi\rho_2/2)}{C_2 \omega^{\rho_2}} \quad (3)$$

$$Z_i = \frac{R_b^2 C_1 \omega^{\rho_1} \sin(\pi\rho_1/2)}{2R_b C_1 \omega^{\rho_1} \cos(\pi\rho_1/2) + R_b^2 C_1^2 \omega^{2\rho_1} + 1} + \frac{\sin(\pi\rho_2/2)}{C_2 \omega^{\rho_2}} \quad (4)$$

The parameters  $C_1$  and  $C_2$  represent the CPE1's capacitance (related to bulk of electrolytes) and CPE2's capacitance (related to electrode-electrolyte interface), respectively. Similarly,  $\rho_1$  and  $\rho_2$  represent the offset from the real and imaginary axes, respectively.

The Nyquist plots in Figure 9 show a typical representation of an EDLC, which shows a semicircle inclined at angle  $\theta$  with the real axis at a high-frequency region and a spike at a low-frequency region. The high-frequency semicircle emanates from the electrode-electrolyte interface while the angle of inclination emanates from the ions' relaxation time. Equation (6) was employed to compute the ionic conductivity of the synthesized SPEs from the bulk resistance [70,71]. The bulk resistance is found from the intercept of the Nyquist plot with the real axis.

$$\sigma = \frac{t}{R_b A} \quad (5)$$

Here,  $t$  stands for the thickness of the film (in cm),  $R_b$  (in  $\Omega$ ) is the film's bulk resistance, and  $A$  is the contact area of the electrode-electrolyte interface (in cm<sup>2</sup>). Table 1a presents the ionic conductivity calculated for different combinations of MC and PVP. Based on the Nyquist plots of the prepared films (Figure S3 in the Supplementary Materials), the bulk resistance decreased as the concentration of PVP decreased. This was due to the plasticizing effect of PVP, which increased the amorphous structure of the polymer blend, as shown in the XRD and FESEM analyses. Additionally, Figures S4 and S5 show that the bulk resistances of the SPE decreased appreciably upon doping with various concentrations of K<sub>2</sub>CO<sub>3</sub> and EC. The increase in ionic conductivity with increasing K<sub>2</sub>CO<sub>3</sub> up to 20 wt.% (Table 1b) could be attributed to CO<sub>3</sub><sup>2-</sup>, which could have plasticized the -C=O...K...O=C- quasi-cross-linking structure in the prepared SPE. A further increase in

$K_2CO_3$  above 20 wt.% caused a sudden decline in ionic conductivity, possibly due to salt ion agglomeration in the polymer matrix [47].

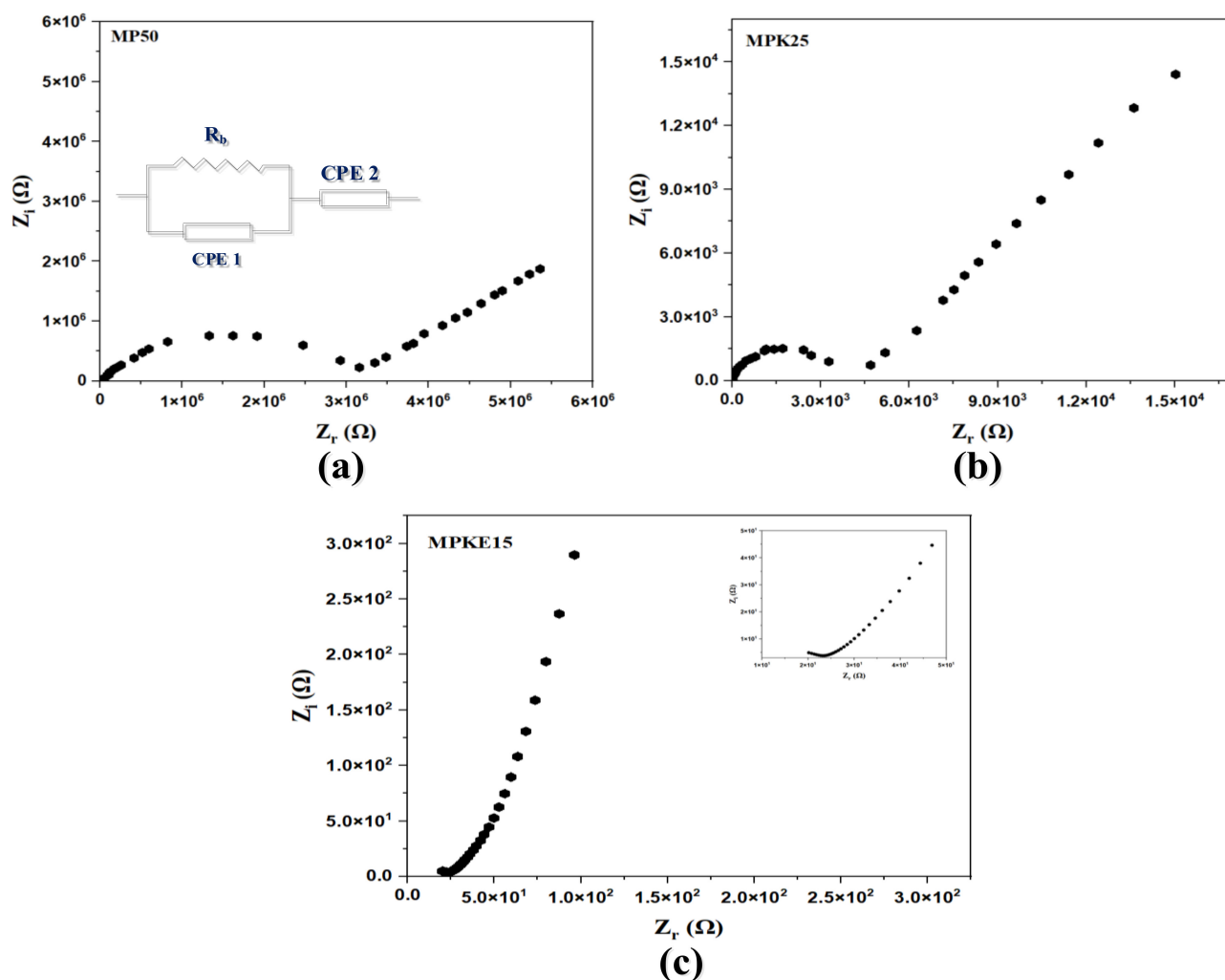


**Figure 9.** Nyquist plots of selected MC/PVP-based SPE with associated ECC. (a) MP50, (b) MPK25 and (c) MPKE15.

When a low-molecular-weight plasticizer is added to a polymer-salt complex, more salt dispersion occurs, which increases the number of charge carriers and boosts the mobility of the polymer-salt complex [22]. In this work, EC (5–25 wt.%) was added to enhance not only the ionic conductivity but also the potential window of the MPK20 system. As seen in Table 1c, the ionic conductivity improved as EC concentrations increased until an optimum conductivity of  $3.88 \times 10^{-4} \text{ Scm}^{-1}$  was attained for the 15 wt.% added sample. The increased conductivity was a result of the EC creating new channels for ions to flow through. Additionally, EC may diminish the Coulombic interaction involving cations and anions. More salts were dissociated into free mobile ions, resulting in an increase in the quantity of ions in the SPE matrix. However, the addition of 20 wt.% or more EC lowered ionic conductivity owing to the displacement of the host polymer by EC molecules inside the salt complexes, resulting in recrystallization of the salt and consequent conductivity reduction.

**Table 1.** (a) Ionic conductivity of MC/PVP polymer blend, (b) ionic conductivity of MC/PVP/K<sub>2</sub>CO<sub>3</sub> SPE, and (c) ionic conductivity of MC/PVP/K<sub>2</sub>CO<sub>3</sub>/EC SPE.

S/N	Sample	Film Thickness × 10 <sup>-3</sup> (cm)	Bulk Resistance (Ohm)	Ionic Conductivity (Scm <sup>-1</sup> )
<b>a</b>				
1.	MP0	9.3	8.97 × 10 <sup>7</sup>	3.30 × 10 <sup>-11</sup>
2.	MP10	9.5	5.31 × 10 <sup>7</sup>	5.71 × 10 <sup>-11</sup>
3.	MP20	9.7	5.14 × 10 <sup>7</sup>	6.01 × 10 <sup>-11</sup>
4.	MP30	9.9	3.33 × 10 <sup>7</sup>	9.45 × 10 <sup>-11</sup>
5.	MP40	9.4	1.56 × 10 <sup>7</sup>	1.92 × 10 <sup>-10</sup>
6.	MP50	9.2	2.98 × 10 <sup>6</sup>	9.83 × 10 <sup>-10</sup>
<b>b</b>				
1.	MPK5	2.33	4.46 × 10 <sup>4</sup>	1.66 × 10 <sup>-7</sup>
2.	MPK10	1.77	2.84 × 10 <sup>4</sup>	1.98 × 10 <sup>-7</sup>
3.	MPK15	2.16	2.13 × 10 <sup>4</sup>	3.23 × 10 <sup>-7</sup>
4.	MPK20	2.21	4.83 × 10 <sup>3</sup>	1.46 × 10 <sup>-6</sup>
5.	MPK25	2.11	4.46 × 10 <sup>4</sup>	1.51 × 10 <sup>-7</sup>
<b>c</b>				
1.	MPKE5	2.62	3.13 × 10 <sup>2</sup>	2.66 × 10 <sup>-5</sup>
2.	MPKE10	2.91	4.94 × 10 <sup>1</sup>	1.87 × 10 <sup>-4</sup>
3.	MPKE15	2.89	2.37 × 10 <sup>1</sup>	3.88 × 10 <sup>-4</sup>
4.	MPKE20	2.74	6.90 × 10 <sup>1</sup>	1.26 × 10 <sup>-4</sup>
5.	MPKE25	2.69	2.16 × 10 <sup>2</sup>	3.98 × 10 <sup>-5</sup>

### 3.4.2. LSV Studies

The electrochemical stability window (ESW) is a critical parameter in SPE technology, particularly for device applications. The LSV approach is used to obtain an approximate breakdown voltage of an electrolyte [72]. Before conducting a charge-discharge cycle test on any device, the electrochemical stability of the sample must be determined because the breakdown voltage is essential for preventing electrolyte destruction. Figure 10 shows the operational stability window of MPK20 and MPKE15 samples investigated in an AUTO-LAB/AUT51018 workstation at a potential range of -2–4 V at a scan rate of 10 mVS<sup>-1</sup>. According to Aziz et al. [52], an electrochemical potential window of 1.27 V is sufficient for a biopolymer electrolyte to be used in EDLC. In this work, the plasticizer-free and EC plasticized samples (MPK20 and MPKE15) recorded a high potential window of 4.35 V and 5.02 V, respectively. Considering the LSV curve of MPKE15, a considerable faradaic current did not appear in the potential range of -3.44 V to 1.57 V. This signifies that the electrolyte system was electrochemically stable across the specified range of potentials [73]. However, when the potential rose beyond 1.57 V, the current increased significantly due to electrolyte breakdown, particularly near the inert electrode's surface. This was due to the decomposition of the SPE.

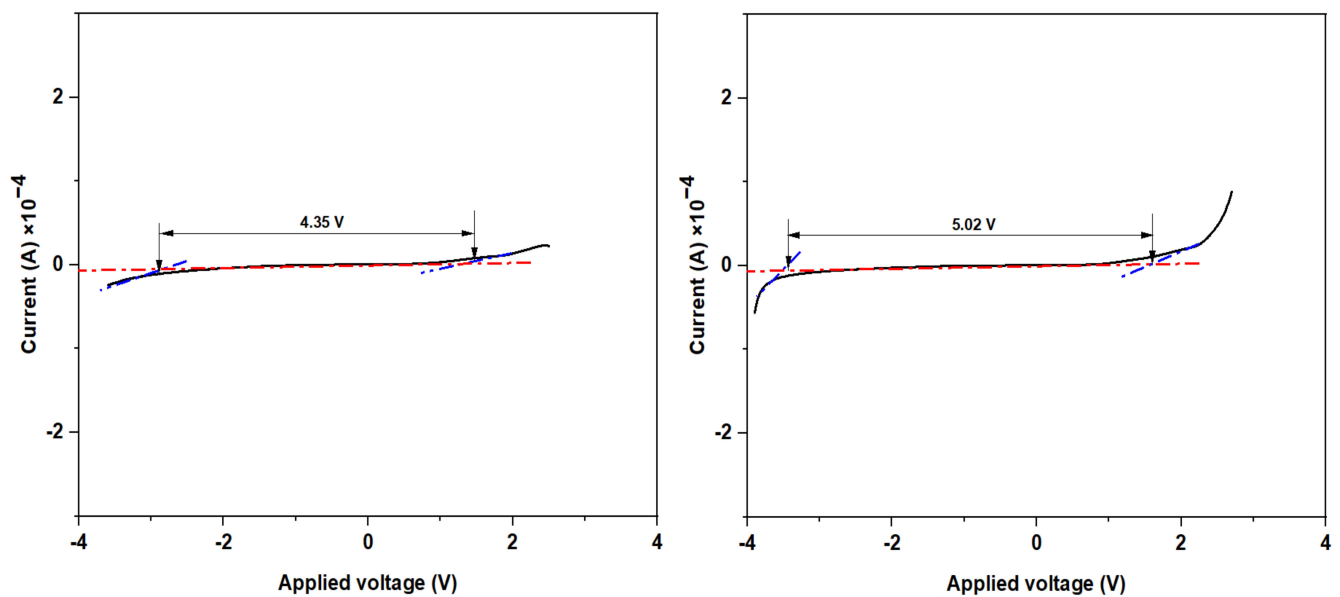


Figure 10. LSV curves of MPK20 and MPKE15 SPE.

### 3.4.3. TNM Measurement

In order to determine if an SPE is suitable for usage in an EDLC, the TNM test may be used. A DC potential was used in this approach, which established the relationship between current and time. At the onset, a high initial current ( $I_i$ ) of 1.781 A was observed, which was due to the contribution of both electrons and ions from an operating voltage of 0.2 V applied to the constructed cell setup. Researchers found that ions are the primary charge carriers in high-conducting electrolyte systems, whereas electrons are the secondary charge carriers [74]. This means the ions contribute more to conductivity. Figure 11 shows the current vs. time plot for the most conducting electrolyte (MPKE15) to discover which charge carrying species are the most prevalent.

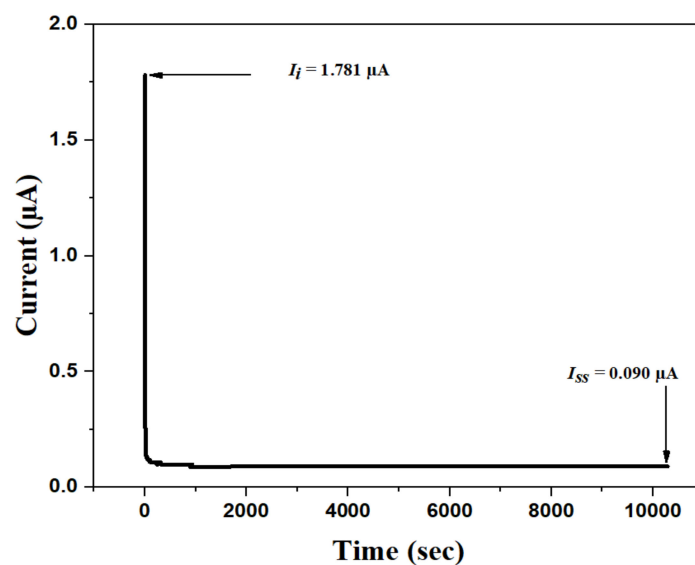


Figure 11. TNM plot of MPKE15 SPE.

Because of the equilibrium between ion diffusion and ion drift at the stainless-steel electrode, a dramatic decrease in current was shown in the polarization plot. As a result, electrons were the only species capable of passing through. Therefore, the steady-state current ( $I_{ss} = 0.090 \mu\text{A}$ ) owing to the electron was reached when all ions in the system were

reduced to zero. In this study, the electron and ion transference numbers ( $t_{el}$  and  $t_{ion}$ ) were determined by using Equations (6) and (7).

$$t_{ion} = \frac{I_i - I_{ss}}{I_i} \quad (6)$$

$$t_{el} = 1 - t_{ion} \quad (7)$$

According to Equation (5), the  $t_{le}$  value is 0.051, whereas the  $t_{ion}$  value is 0.949 (obtained from Equation (6)). Obviously, the high  $t_{ion}$  value obtained, which is near to the ideal value of one, demonstrates the ionic nature of the charge transfer mechanism inside the SPE. To better appreciate the results obtained in this study, we compared the performance of MPKE15 with some related work previously reported. As can be seen in Table 2, this work outperformed previous works in terms of collective electrochemical properties.

**Table 2.** Comparison of electrochemical performance of selected SPEs.

Polymer-Salt Complex	RT Ionic Conductivity (Scm <sup>-1</sup> )	Potential Window (V)	Ion Transference Number	Ref.
CS/DX/NH <sub>4</sub> PF <sub>6</sub> /glycerol	3.0 × 10 <sup>-4</sup>	1.5	0.96	[75]
CS/MC/NH <sub>4</sub> NO <sub>3</sub> /glycerol	1.31 × 10 <sup>-4</sup>	1.87	0.93	[22]
CS/MC/NH <sub>4</sub> I	1.93 × 10 <sup>-4</sup>	2.10	0.93	[76]
MC/PC/K <sub>3</sub> PO <sub>4</sub> /glycerol	3.0 × 10 <sup>-4</sup>	4.19	-	[6]
MC/PC/NH <sub>4</sub> Cl/ZnO	3.13 × 10 <sup>-4</sup>	4.55	-	[66]
DX/CS/NaF/glycerol	6.10 × 10 <sup>-5</sup>	2.55	0.99	[69]
PVA/CS/NH <sub>4</sub> SCN	1.36 × 10 <sup>-5</sup>	2.25	0.72	[77]
MC/PVP/K <sub>2</sub> CO <sub>3</sub> /EC	3.88 × 10 <sup>-4</sup>	5.02	0.949	This work

RT = room temperature.

### 3.5. Device Study

#### CV Analysis

Figure 12 illustrates the effect of a scan rate on the primary characteristic of the CV profile with no noticeable redox peak throughout the voltage range. The CV displays a leaf-like pattern at every scan rate. An ideal EDLC is defined by the presence of a rectangular CV electrochemical characteristic [78]. In essence, however, the primary characteristics of CV obtained in this study were altered owing to the nature of the electrode surface (porosity), which caused variations in internal resistance. This change in CV response influenced both the performance and efficiency of the EDLC [3]. Furthermore, the absence of redox peaks in the CV profile demonstrated the occurrence of a charge-storing capability through a non-faradaic process, which is a fundamental property of a true EDLC. In accordance with this method, both cations' and anions' adsorption and desorption occurred at the electrode surfaces; in other words, intercalation and deintercalation processes were absent [79].

The CV values at various scan rates are shown in Table 3, where the greatest value is observed at a low scan rate and declines progressively as the scan rate rises. In theory, at a low scan rate, a stable double-layer charge occurs at the interface due to the adsorption of ions [80]. Obviously, a nearly perfect plateau obtained at low scan rates is due to the formation of a broad diffusion layer at the interface as a result of ion adsorption. This phenomenon also results in low ohmic resistance at lower scan rates. At a fast scan rate, on the other hand, a narrow, diffusion layer is generated, resulting in a low capacitance [3].

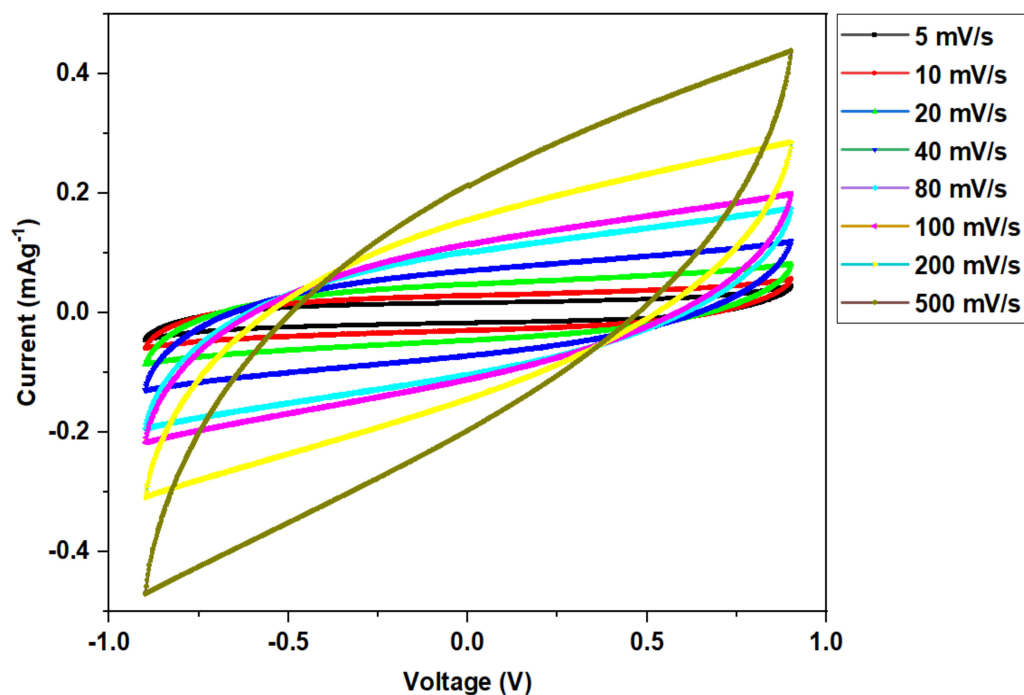


Figure 12. The CV profile for the fabricated EDLC cell at various scan rates.

Table 3. Variation of specific capacitance at different scan rates for the fabricated EDLC.

Scan Rate ( $\text{mVs}^{-1}$ )	Specific Capacitance ( $\text{Fg}^{-1}$ )
5	54.936
10	45.849
20	36.065
40	26.797
80	18.936
100	16.600
200	10.897
500	5.923

#### 4. Conclusions

In this work, MC/PVP/ $\text{K}_2\text{CO}_3$ -based SPE with added EC as plasticizer showed excellent electrochemical properties and, therefore, its viability as a green and sustainable replacement electrolyte. The SPE system was also able to match the performance of some existing green and sustainable SPEs. Various methods, such as XRD, FTIR, EIS, SV, and TNM, were used to examine the polymer samples' structural and electrical characteristics. Molecular interactions between PVP and PVC were seen in the changing FTIR band peaks, which indicate a successful blending of the two polymers. Crystallinity was reduced when the PVP content was increased in the MC/PVP blend system. The presence and shift of identified functional groups in the FTIR study demonstrated the creation of an MC/PVP/ $\text{K}_2\text{CO}_3$  complex and that EC interacted with this complex. The MPKE15 doped with 15% EC (MPKE15) had the greatest room temperature conductivity of  $3.88 \times 10^{-4} \text{ Scm}^{-1}$  with a potential window of 5.02 V. According to the LSV study, the breakdown of the film occurred at potentials greater than 5.02 V, and the sample exhibited stability throughout a broad range of potential windows. As per the TNM study, the  $t_{ion}$  value for MPKE15 was 0.949 but the  $t_{el}$  value was 0.051. Using the optimum sample (MPKE15), an EDLC was fabricated and the CV profile of the EDLC recorded a specific capacitance of  $54.936 \text{ Fg}^{-1}$  at  $5 \text{ mVs}^{-1}$ .

**Supplementary Materials:** The following supporting information can be downloaded at <https://www.mdpi.com/article/10.3390/polym14153055/s1>. Figure S1: (a) Pure PVP film stuck to the petri dish, (b) FESEM image of pure PVP film on petri dish substrate. Figure S2: Images of SPEs under different manipulations. Figure S3: Nyquist plots of MC/PVP polymer blend samples. Figure S4: Nyquist plots of other MC/PVP/K<sub>2</sub>CO<sub>3</sub> SPEs. Figure S5: Nyquist plots of other MC/PVP/K<sub>2</sub>CO<sub>3</sub>/EC SPEs. Table S1: Band assignment for MC/PVP polymer blend. References [81–85] are cited in the Supplementary Materials.

**Author Contributions:** Conceptualization, A.A.A., M.F.B.A.S., H.S. and J.O.D.; methodology, A.A.A., A.B.A. and M.K.M.A.; validation, J.O.D., O.A.A. and K.H.I.; formal analysis, A.A.A., K.H.I., H.S., M.F.B.A.S. and O.A.A. investigation, A.A.A., A.B.A., M.F.B.A.S. and H.S.; resources, M.K.M.A., K.H.I., O.A.A., N.F.M.A.A. and M.A.I. writing—original draft preparation, A.A.A.; writing—review and editing, A.A.A., J.O.D., M.F.B.A.S. and H.S.; visualization, A.A.A., O.A.A., M.F.B.A.S., N.F.M.A.A. and H.S.; funding acquisition, J.O.D., M.K.M.A., O.A.A. and K.H.I. All authors have read and agreed to the published version of the manuscript.

**Funding:** The Deanship of Scientific Research at Imam Mohammad Ibn Saud Islamic University Research Group no. RG-21-09-48.

**Institutional Review Board Statement:** Not applicable.

**Informed Consent Statement:** Not applicable.

**Data Availability Statement:** The data presented in this study are available on request from the corresponding author. The data are not publicly available due to privacy.

**Acknowledgments:** The authors extend their appreciation to the Deanship of Scientific Research at Imam Mohammad Ibn Saud Islamic University for funding this work through Research Group no. RG-21-09-48 and the Universiti Teknologi PETRONAS, Malaysia, for providing research facilities.

**Conflicts of Interest:** The authors declare no conflict of interest.

## References

1. Putri, R.M.; Sundari, C.D.D.; Floweri, O.; Mayangsari, T.R.; Ivansyah, A.L.; Santosa, S.P.; Arcana, I.M.; Iskandar, F. PEO/PVA/LiOH Solid Polymer Electrolyte Prepared via Ultrasound-assisted Solution Cast Method. *J. Non-Cryst. Solids* **2021**, *556*, 120549. [[CrossRef](#)]
2. Javed, K.; Oolo, M.; Savest, N.; Krumme, A. A review on graphene-based electrospun conductive nanofibers, supercapacitors, anodes, and cathodes for lithium-ion batteries. *Crit. Rev. Solid State Mater. Sci.* **2019**, *44*, 427–443. [[CrossRef](#)]
3. Dannoun, E.M.; Aziz, S.B.; Brza, M.A.; Nofal, M.M.; Asnawi, A.S.; Yusof, Y.M.; Al-Zangana, S.; Hamsan, M.H.; Kadir, M.F.Z.; Woo, H.J. The Study of Plasticized Solid Polymer Blend Electrolytes Based on Natural Polymers and Their Application for Energy Storage EDLC Devices. *Polymers* **2020**, *12*, 2531. [[CrossRef](#)] [[PubMed](#)]
4. Adam, A.A.; Ojur Dennis, J.; Al-Hadeethi, Y.; Mkawi, E.M.; Abubakar Abdulkadir, B.; Usman, F.; Mudassir Hassan, Y.; Wadi, I.A.; Sani, M. State of the Art and New Directions on Electrospun Lignin/Cellulose Nanofibers for Supercapacitor Application: A Systematic Literature Review. *Polymers* **2020**, *12*, 2884. [[CrossRef](#)]
5. Mahalakshmi, M.; Selvanayagam, S.; Selvasekarapandian, S.; Chandra, M.V.L.; Sangeetha, P.; Manjuladevi, R. Magnesium ion-conducting solid polymer electrolyte based on cellulose acetate with magnesium nitrate (Mg(NO<sub>3</sub>)<sub>2</sub>·6H<sub>2</sub>O) for electrochemical studies. *Ionics* **2020**, *26*, 4553–4565. [[CrossRef](#)]
6. Adam, A.A.; Soleimani, H.; Shukur, M.F.B.A.; Dennis, J.O.; Abdulkadir, B.A.; Hassan, Y.M.; Yusuf, J.Y.; Shamsuri, N.A.B. A new approach to understanding the interaction effect of salt and plasticizer on solid polymer electrolytes using statistical model and artificial intelligence algorithm. *J. Non-Cryst. Solids* **2022**, *587*, 121597. [[CrossRef](#)]
7. Nadirah, B.N.; Ong, C.C.; Saheed, M.S.M.; Yusof, Y.M.; Shukur, M.F. Structural and conductivity studies of polyacrylonitrile/methylcellulose blend based electrolytes embedded with lithium iodide. *Int. J. Hydrogen Energy* **2020**, *45*, 19590–19600. [[CrossRef](#)]
8. Xu, L.; Li, J.; Deng, W.; Li, L.; Zou, G.; Hou, H.; Huang, L.; Ji, X. Boosting the ionic conductivity of PEO electrolytes by waste eggshell-derived fillers for high-performance solid lithium/sodium batteries. *Mater. Chem. Front.* **2021**, *5*, 1315–1323. [[CrossRef](#)]
9. Hassan, Y.M.; Guan, B.H.; Zaid, H.M.; Hamza, M.F.; Adil, M.; Adam, A.A.; Hastuti, K. Application of Magnetic and Dielectric Nanofluids for Electromagnetic-Assistance Enhanced Oil Recovery: A Review. *Crystals* **2021**, *11*, 106. [[CrossRef](#)]
10. Hassan, Y.M.; Guan, B.H.; Chuan, L.K.; Zaid, H.M.; Hamza, M.F.; Adam, A.A.; Usman, F.; Oluwatobi, Y.A. Effect of annealing temperature on the rheological property of ZnO/SiO<sub>2</sub> nanocomposites for Enhanced Oil Recovery. *Mater. Today Proc.* **2022**, *48*, 905–910. [[CrossRef](#)]

11. Hassan, Y.M.; Guan, B.H.; Chuan, L.K.; Khandaker, M.U.; Sikiru, S.; Halilu, A.; Adam, A.A.; Abdulkadir, B.A.; Usman, F. Electromagnetically Modified Wettability and Interfacial Tension of Hybrid ZnO/SiO<sub>2</sub> Nanofluids. *Crystals* **2022**, *12*, 169. [[CrossRef](#)]
12. Hassan, Y.M.; Guan, B.H.; Chuan, L.K.; Halilu, A.; Adil, M.; Adam, A.A.; Abdulkadir, B.A. Interfacial tension and wettability of hybridized ZnOFe<sub>2</sub>O<sub>3</sub>/SiO<sub>2</sub> based nanofluid under electromagnetic field inducement. *J. Pet. Sci. Eng.* **2022**, *211*, 110184. [[CrossRef](#)]
13. Hassan, Y.M.; Guan, B.H.; Chuan, L.K.; Hamza, M.F.; Khandaker, M.U.; Sikiru, S.; Adam, A.A.; Abdul Sani, S.F.; Abdulkadir, B.A.; Ayub, S. The influence of ZnO/SiO<sub>2</sub> nanocomposite concentration on rheology, interfacial tension, and wettability for enhanced oil recovery. *Chem. Eng. Res. Des.* **2022**, *179*, 452–461. [[CrossRef](#)]
14. Hassan, Y.M.; Guan, B.H.; Chuan, L.K.; Hamza, M.F.; Adil, M.; Adam, A.A. The synergistic effect of Fe<sub>2</sub>O<sub>3</sub>/SiO<sub>2</sub> nanoparticles concentration on rheology, wettability, and brine-oil interfacial tension. *J. Pet. Sci. Eng.* **2022**, *210*, 110059. [[CrossRef](#)]
15. Mathela, S.; Sangwan, B.; Dhapola, P.S.; Singh, P.K.; Tomar, R. Ionic liquid incorporated poly (ethylene oxide) (PEO) doped with potassium iodide (KI) solid polymer electrolyte for energy device. *Mater. Today Proc.* **2022**, *49*, 3250–3253. [[CrossRef](#)]
16. Hamsan, M.H.; Shukur, M.F.; Aziz, S.B.; Yusof, Y.M.; Kadir, M.F.Z. Influence of NH<sub>4</sub>Br as an ionic source on the structural/electrical properties of dextran-based biopolymer electrolytes and EDLC application. *Bull. Mater. Sci.* **2019**, *43*, 30. [[CrossRef](#)]
17. Shuhaimi, N.E.A.; Teo, L.P.; Majid, S.R.; Arof, A.K. Transport studies of NH<sub>4</sub>NO<sub>3</sub> doped methyl cellulose electrolyte. *Synth. Met.* **2010**, *160*, 1040–1044. [[CrossRef](#)]
18. Asnawi, A.; Hamsan, M.; Kadir, M.; Aziz, S.; Yusof, Y.J.M.C.; Crystals, L. Investigation on electrochemical characteristics of maltodextrin–methyl cellulose electrolytes. *Mol. Cryst. Liq. Cryst.* **2020**, *708*, 63–91. [[CrossRef](#)]
19. Abdullah, S.; Ahmad, A.S.; Latif, K.S.A.; Sobri, N.A.M.; Abdullah, N.; Hashim, N.; Yahya, N.M.; Mohamed, R.M. Characterization of Solid Polymer Electrolyte Membrane made of Methylcellulose and Ammonium Nitrate. *J. Phys. Conf. Ser.* **2020**, *1532*, 012017. [[CrossRef](#)]
20. Ahmed, H.T.; Abdullah, O.G. Impedance and ionic transport properties of proton-conducting electrolytes based on polyethylene oxide/methylcellulose blend polymers. *J. Sci. Adv. Mater. Devices* **2020**, *5*, 125–133. [[CrossRef](#)]
21. Shamsuri, N.A.; Zaine, S.N.A.; Yusof, Y.M.; Yahya, W.Z.N.; Shukur, M.F. Effect of ammonium thiocyanate on ionic conductivity and thermal properties of polyvinyl alcohol–methylcellulose–based polymer electrolytes. *Ionics* **2020**, *26*, 6083–6093. [[CrossRef](#)]
22. Aziz, S.B.; Dannoun, E.; Hamsan, M.H.; Ghareeb, H.O.; Nofal, M.M.; Karim, W.O.; Asnawi, A.S.; Hadi, J.M.; Kadir, M. A Polymer Blend Electrolyte Based on CS with Enhanced Ion Transport and Electrochemical Properties for Electrical Double Layer Capacitor Applications. *Polymers* **2021**, *13*, 930. [[CrossRef](#)]
23. Asnawi, A.S.F.M.; Hamsan, M.H.; Aziz, S.B.; Kadir, M.F.Z.; Matmin, J.; Yusof, Y.M. Impregnation of [Emim]Br ionic liquid as plasticizer in biopolymer electrolytes for EDLC application. *Electrochim. Acta* **2021**, *375*, 137923. [[CrossRef](#)]
24. Hamsan, M.; Aziz, S.B.; Shukur, M.; Kadir, M.J.I. Protonic cell performance employing electrolytes based on plasticized methylcellulose–potato starch–NH<sub>4</sub>NO. *Ionics* **2019**, *25*, 559–572. [[CrossRef](#)]
25. Fan, L.; Wang, M.; Zhang, Z.; Qin, G.; Hu, X.; Chen, Q. Preparation and Characterization of PVA Alkaline Solid Polymer Electrolyte with Addition of Bamboo Charcoal. *Materials* **2018**, *11*, 679. [[CrossRef](#)] [[PubMed](#)]
26. Sunitha, V.; Kabbur, S.K.M.; Pavan, G.; Sandesh, N.; Suhas, M.; Lalithnarayan, C.; Laxman, N.; Radhakrishnan, S.J.I. Lithium ion conduction in PVA-based polymer electrolyte system modified with combination of nanofillers. *Ionics* **2020**, *26*, 823–829. [[CrossRef](#)]
27. Saeed, M.A.M.; Abdullah, O.G. Effect of High Ammonium Salt Concentration and Temperature on the Structure, Morphology, and Ionic Conductivity of Proton-Conductor Solid Polymer Electrolytes Based PVA. *Membranes* **2020**, *10*, 262. [[CrossRef](#)] [[PubMed](#)]
28. Liu, J.; Khanam, Z.; Muchakayala, R.; Song, S. Fabrication and characterization of Zn-ion-conducting solid polymer electrolyte films based on PVdF–HFP/Zn(Tf)<sub>2</sub> complex system. *J. Mater. Sci. Mater. Electron.* **2020**, *31*, 6160–6173. [[CrossRef](#)]
29. Sedlak, P.; Gajdos, A.; Macku, R.; Majzner, J.; Holcman, V.; Sedlakova, V.; Kubersky, P.J.S.R. The effect of thermal treatment on ac/dc conductivity and current fluctuations of PVDF/NMP/[EMIM][TFSI] solid polymer electrolyte. *Sci. Rep.* **2020**, *10*, 21140. [[CrossRef](#)]
30. Han, L.; Wang, J.; Mu, X.; Wu, T.; Liao, C.; Wu, N.; Xing, W.; Song, L.; Kan, Y.; Hu, Y. Controllable magnetic field aligned sepiolite nanowires for high ionic conductivity and high safety PEO solid polymer electrolytes. *J. Colloid Interface Sci.* **2021**, *585*, 596–604. [[CrossRef](#)]
31. Wen, J.; Zhao, Q.; Jiang, X.; Ji, G.; Wang, R.; Lu, G.; Long, J.; Hu, N.; Xu, C. Graphene Oxide Enabled Flexible PEO-Based Solid Polymer Electrolyte for All-Solid-State Lithium Metal Battery. *ACS Appl. Energy Mater.* **2021**, *4*, 3660–3669. [[CrossRef](#)]
32. Jothi, M.A.; Vanitha, D.; Nallamuthu, N.; Manikandan, A.; Bahadur, S.A. Investigations of lithium ion conducting polymer blend electrolytes using biodegradable cornstarch and PVP. *Phys. B Condens. Matter* **2020**, *580*, 411940. [[CrossRef](#)]
33. Sangwan, B.; Mathela, S.; Dhapola, P.S.; Singh, P.K.; Tomar, R. Ionic liquid incorporated polyvinylpyrrolidone (PVP) doped with ammonium iodide (NH<sub>4</sub>I) doped solid polymer electrolyte for energy device. *Mater. Today Proc.* **2021**, *49*, 3306–3309. [[CrossRef](#)]
34. Saeed, A.M.N.; Hezam, A.; Al-Gunaid, M.Q.A.; TE, S.; Siddaramaiah. Effect of ethylene carbonate on properties of PVP–CsAlO<sub>2</sub>–LiClO<sub>4</sub> solid polymer electrolytes. *Polym.-Plast. Technol. Mater.* **2021**, *60*, 132–146. [[CrossRef](#)]

35. Sreekanth, K.; Siddaiah, T.; Gopal, N.O.; Madhava Kumar, Y.; Ramu, C. Thermal, structural, optical and electrical conductivity studies of pure and Fe<sup>3+</sup> ions doped PVP films for semiconducting polymer devices. *Mater. Res. Innov.* **2021**, *25*, 95–103. [[CrossRef](#)]
36. Jothi, M.A.; Vanitha, D.; Bahadur, S.A.; Nallamuthu, N. Proton conducting polymer electrolyte based on cornstarch, PVP, and NH<sub>4</sub>Br for energy storage applications. *Ionics* **2021**, *27*, 225–237. [[CrossRef](#)]
37. Sadiq, M.; Raza, M.M.H.; Murtaza, T.; Zulfeqar, M.; Ali, J. Sodium Ion-Conducting Polyvinylpyrrolidone (PVP)/Polyvinyl Alcohol (PVA) Blend Electrolyte Films. *J. Electron. Mater.* **2021**, *50*, 403–418. [[CrossRef](#)]
38. Nofal, M.M.; Hadi, J.M.; Aziz, S.B.; Brza, M.A.; Asnawi, A.; Dannoun, E.M.A.; Abdullah, A.M.; Kadir, M.F.Z. A Study of Methylcellulose Based Polymer Electrolyte Impregnated with Potassium Ion Conducting Carrier: Impedance, EEC Modeling, FTIR, Dielectric, and Device Characteristics. *Materials* **2021**, *14*, 4859. [[CrossRef](#)]
39. Adam, A.A.; Ramamurthi, K.; Margoni, M.M. A Study on Low Cost-Highly Transparent and Conductive Molybdenum Doped Zinc Oxide Thin Films Deposited by Spray Pyrolysis Technique. *Am. J. Mater. Res.* **2018**, *5*, 40–45.
40. Adam, A.A.; Musa, M.; Sani, M. Enhanced optical transmittance of spray deposited zinc oxide thin films for optoelectronic applications. *Bayero J. Pure Appl. Sci.* **2020**, *12*, 1–5. [[CrossRef](#)]
41. Abdulkadir, B.A.; Dennis, J.O.; Shukur, M.F.B.A.; Nasef, M.M.E.; Usman, F. Preparation and characterization of gel polymer electrolyte based on PVA-K<sub>2</sub>CO<sub>3</sub>. *Polym.-Plast. Technol. Mater.* **2020**, *59*, 1679–1697.
42. Dhanasekaran, P.; Lokesh, K.; Ojha, P.K.; Sahu, A.K.; Bhat, S.D.; Kalpana, D. Electrochemical deposition of three-dimensional platinum nanoflowers for high-performance polymer electrolyte fuel cells. *J. Colloid Interface Sci.* **2020**, *572*, 198–206. [[CrossRef](#)]
43. Khoon, L.T.; Fui, M.-L.W.; Hassan, N.H.; Su'ait, M.S.; Vedarajan, R.; Matsumi, N.; Bin Kassim, M.; Shyuan, L.K.; Ahmad, A. In situ sol-gel preparation of ZrO<sub>2</sub> in nano-composite polymer electrolyte of PVDF-HFP/MG49 for lithium-ion polymer battery. *J. Sol-Gel Sci. Technol.* **2019**, *90*, 665–675. [[CrossRef](#)]
44. Mallaiyah, Y.; Jeedi, V.R.; Swarnalatha, R.; Raju, A.; Narender Reddy, S.; Sadananda Chary, A. Impact of polymer blending on ionic conduction mechanism and dielectric properties of sodium based PEO-PVdF solid polymer electrolyte systems. *J. Phys. Chem. Solids* **2021**, *155*, 110096. [[CrossRef](#)]
45. Ramesh, S.; Lu, S.-C.; Morris, E. Towards magnesium ion conducting poly(vinylidene fluoride-hexafluoropropylene)-based solid polymer electrolytes with great prospects: Ionic conductivity and dielectric behaviours. *J. Taiwan Inst. Chem. Eng.* **2012**, *43*, 806–812. [[CrossRef](#)]
46. Abdulkadir, B.A.; Ojur Dennis, J.; Al-Hadeethi, Y.; Shukur, M.F.B.A.; Mkawi, E.M.; Al-Harbi, N.; Ibnaouf, K.H.; Aldaghri, O.; Usman, F.; Abbas Adam, A. Optimization of the Electrochemical Performance of a Composite Polymer Electrolyte Based on PVA-K<sub>2</sub>CO<sub>3</sub>-SiO<sub>2</sub> Composite. *Polymers* **2020**, *13*, 92. [[CrossRef](#)]
47. Hamsan, M.H.; Shukur, M.F.; Kadir, M.F.Z. The effect of NH<sub>4</sub>NO<sub>3</sub> towards the conductivity enhancement and electrical behavior in methyl cellulose-starch blend based ionic conductors. *Ionics* **2016**, *23*, 1137–1154. [[CrossRef](#)]
48. Kadir, M.F.Z.; Salleh, N.S.; Hamsan, M.H.; Aspanut, Z.; Majid, N.A.; Shukur, M.F. Biopolymeric electrolyte based on glycerolized methyl cellulose with NH<sub>4</sub>Br as proton source and potential application in EDLC. *Ionics* **2018**, *24*, 1651–1662. [[CrossRef](#)]
49. Nofal, M.M.; Aziz, S.B.; Brza, M.A.; Abdullah, S.N.; Dannoun, E.M.A.; Hadi, J.M.; Murad, A.R.; Al-Saeedi, S.I.; Kadir, M.F.Z. Studies of Circuit Design, Structural, Relaxation and Potential Stability of Polymer Blend Electrolyte Membranes Based on PVA:MC Impregnated with NH<sub>4</sub>I Salt. *Membranes* **2022**, *12*, 284. [[CrossRef](#)]
50. Abdullah, O.G.; Aziz, S.B.; Rasheed, M.A. Structural and optical characterization of PVA:KMnO<sub>4</sub> based solid polymer electrolyte. *Results Phys.* **2016**, *6*, 1103–1108. [[CrossRef](#)]
51. Salehan, S.S.; Nadirah, B.N.; Saheed, M.S.M.; Yahya, W.Z.N.; Shukur, M.F. Conductivity, structural and thermal properties of corn starch-lithium iodide nanocomposite polymer electrolyte incorporated with Al<sub>2</sub>O<sub>3</sub>. *J. Polym. Res.* **2021**, *28*, 222. [[CrossRef](#)]
52. Aziz, S.B.; Brza, M.; Mishra, K.; Hamsan, M.; Karim, W.O.; Abdullah, R.M.; Kadir, M.; Abdulwahid, R.T. Fabrication of high performance energy storage EDLC device from proton conducting methylcellulose: Dextran polymer blend electrolytes. *J. Mater. Res. Technol.* **2020**, *9*, 1137–1150. [[CrossRef](#)]
53. Rahamathullah, R.; Khairul, W.M.; Isa, M.I.N. Contribution of stilbene-imine additives on the structural, ionic conductivity performance and theoretical evaluation on CMC-based biopolymer electrolytes. *Carbohydr. Polym.* **2020**, *250*, 116935. [[CrossRef](#)] [[PubMed](#)]
54. Saadiah, M.A.; Nagao, Y.; Samsudin, A.S. Enhancement on protonation (H<sup>+</sup>) with incorporation of flexible ethylene carbonate in CMC-PVA-30 wt.% NH<sub>4</sub>NO<sub>3</sub> film. *Int. J. Hydrogen Energy* **2021**, *46*, 17231–17245. [[CrossRef](#)]
55. Abdulkadir, B.A.; Dennis, J.O.; Adam, A.A.; Al-Dhahebi, A.M.; Shukur, M.F. Novel electrospun separator-electrolyte based on PVA-K<sub>2</sub>CO<sub>3</sub>-SiO<sub>2</sub>-cellulose nanofiber for application in flexible energy storage devices. *J. Appl. Polym. Sci.* **2022**, *139*, 52308. [[CrossRef](#)]
56. Alves, R.; Sentanin, F.; Sabadini, R.C.; Pawlicka, A.; Silva, M.M. Innovative electrolytes based on chitosan and thulium for solid state applications: Synthesis, structural, and thermal characterization. *J. Electroanal. Chem.* **2017**, *788*, 156–164. [[CrossRef](#)]
57. Ait Hana, N.; Aride, J.; Haddad, M.; Benkhoucha, K.; Sahraoui, B.; Taibi, M. Electrical and structural analysis of xPbO-(1-x)B<sub>2</sub>O<sub>3</sub> (0.3 ≤ x ≤ 0.9) glasses. *Mol. Cryst. Liq. Cryst.* **2016**, *627*, 106–117. [[CrossRef](#)]
58. Pandi, D.V.; Selvasekarapandian, S.; Bhuvaneswari, R.; Premalatha, M.; Monisha, S.; Arunkumar, D.; Junichi, K. Development and characterization of proton conducting polymer electrolyte based on PVA, amino acid glycine and NH<sub>4</sub>SCN. *Solid State Ionics* **2016**, *298*, 15–22. [[CrossRef](#)]

59. Long, M.-C.; Xia, L.-T.; Lyu, T.-B.; Wang, T.; Huang, T.; Chen, L.; Wu, G.; Wang, X.-L.; Wang, Y.-Z. A green and facile way to prepare methylcellulose-based porous polymer electrolytes with high lithium-ion conductivity. *Polymer* **2019**, *176*, 256–263. [[CrossRef](#)]
60. Nurhaziqah, A.M.S.; Afifah, I.Q.; Aziz, M.F.H.A.; Aziz, N.A.N.; Hasiah, S. Optical, Structural and Electrical Studies of Biopolymer Electrolytes Based on Methylcellulose Doped with Ca(NO<sub>3</sub>). *IOP Conf. Ser. Mater. Sci. Eng.* **2018**, *440*, 012034. [[CrossRef](#)]
61. Anilkumar, K.M.; Jinisha, B.; Manoj, M.; Jayalekshmi, S. Poly(ethylene oxide) (PEO)—Poly(vinyl pyrrolidone) (PVP) blend polymer based solid electrolyte membranes for developing solid state magnesium ion cells. *Eur. Polym. J.* **2017**, *89*, 249–262. [[CrossRef](#)]
62. Zhang, L.; Wang, X.F.; Peng, Y.L.; Zhao, Y.; Qian, J.Y.; Ding, X. Effect of different ionic liquids acting as plasticizers on the multi-scale structures and physical properties of hydroxypropyl methylcellulose/monosodium phosphate photophobic film. *Int. J. Biol. Macromol.* **2021**, *179*, 466–474. [[CrossRef](#)]
63. Genier, F.S.; Burdin, C.V.; Biria, S.; Hosein, I.D. A novel calcium-ion solid polymer electrolyte based on crosslinked poly(ethylene glycol) diacrylate. *J. Power Sources* **2019**, *414*, 302–307. [[CrossRef](#)]
64. Kiruthika, S.; Malathi, M.; Selvasekarapandian, S.; Tamilarasan, K.; Maheshwari, T. Conducting biopolymer electrolyte based on pectin with magnesium chloride salt for magnesium battery application. *Polym. Bull.* **2020**, *77*, 6299–6317. [[CrossRef](#)]
65. Mustapa, S.R.; Aung, M.M.; Rayung, M. Physico-Chemical, Thermal, and Electrochemical Analysis of Solid Polymer Electrolyte from Vegetable Oil-Based Polyurethane. *Polymers* **2021**, *13*, 132. [[CrossRef](#)]
66. Dennis, J.O.; Adam, A.A.; Ali, M.K.M.; Soleimani, H.; Shukur, M.F.B.A.; Ibnaouf, K.H.; Aldaghri, O.; Eisa, M.H.; Ibrahim, M.A.; Bashir Abdulkadir, A.; et al. Substantial Proton Ion Conduction in Methylcellulose/Pectin/Ammonium Chloride Based Solid Nanocomposite Polymer Electrolytes: Effect of ZnO Nanofiller. *Membranes* **2022**, *12*, 706. [[CrossRef](#)]
67. Tuan Naiwi, T.S.R.; Aung, M.M.; Ahmad, A.; Rayung, M.; Su'ait, M.S.; Yusof, N.A.; Wynn Lae, K.Z. Enhancement of Plasticizing Effect on Bio-Based Polyurethane Acrylate Solid Polymer Electrolyte and Its Properties. *Polymers* **2018**, *10*, 1142. [[CrossRef](#)]
68. Feng, X.; Liu, Q.; Zheng, J.; Xu, Y.; Chen, W. Poly(ethylene oxide)-ethylene carbonate solid binary electrolyte with higher conductivity, lower operating temperature and fully impregnated separator for all solid-state lithium ion batteries. *Compos. Commun.* **2022**, *29*, 101026. [[CrossRef](#)]
69. Asnawi, A.S.F.M.; Aziz, S.B.; Brevik, I.; Brza, M.A.; Yusof, Y.M.; Alshehri, S.M.; Ahamad, T.; Kadir, M.F.Z. The Study of Plasticized Sodium Ion Conducting Polymer Blend Electrolyte Membranes Based on Chitosan/Dextran Biopolymers: Ion Transport, Structural, Morphological and Potential Stability. *Polymers* **2021**, *13*, 383. [[CrossRef](#)]
70. Aziz, S.B.; Faraj, M.; Abdullah, O.G. Impedance spectroscopy as a novel approach to probe the phase transition and microstructures existing in CS: PEO based blend electrolytes. *Sci. Rep.* **2018**, *8*, 14308. [[CrossRef](#)]
71. Abdulkadir, B.A.; Dennis, J.O.; Abd Shukur, M.F.B.; Nasef, M.M.E.; Usman, F.; Adam, A.A.; Adamu, U.A. Dielectric Study of Gel Polymer Electrolyte Based on PVA-K<sub>2</sub>CO<sub>3</sub>-SiO. *IOP Conf. Ser. Mater. Sci. Eng.* **2021**, *1092*, 012066. [[CrossRef](#)]
72. Kamboj, V.; Arya, A.; Tanwar, S.; Kumar, V.; Sharma, A.L. Nanofiller-assisted Na<sup>+</sup>-conducting polymer nanocomposite for ultracapacitor: Structural, dielectric and electrochemical properties. *J. Mater. Sci.* **2021**, *56*, 6167–6187. [[CrossRef](#)]
73. Dannoun, E.M.A.; Aziz, S.B.; Kadir, M.F.Z.; Brza, M.A.; Nofal, M.M.; Hadi, J.M.; Al-Saeedi, S.I.; Abdulwahid, R.T. The study of impedance, ion transport properties, EEC modeling, dielectric and electrochemical characteristics of plasticized proton conducting PVA based electrolytes. *J. Mater. Res. Technol.* **2022**, *17*, 1976–1985. [[CrossRef](#)]
74. Abdulkareem, S.S. Structural, morphological and electrical properties of chitosan/methylcellulose blend polymer doped with different concentrations of NH<sub>4</sub>NO. *Mater. Res. Express* **2021**, *8*, 086301. [[CrossRef](#)]
75. Aziz, S.B.; Brza, M.A.; Brevik, I.; Hafiz, M.H.; Asnawi, A.S.F.M.; Yusof, Y.M.; Abdulwahid, R.T.; Kadir, M.F.Z. Blending and Characteristics of Electrochemical Double-Layer Capacitor Device Assembled from Plasticized Proton Ion Conducting Chitosan:Dextran:NH<sub>4</sub>PF<sub>6</sub> Polymer Electrolytes. *Polymers* **2020**, *12*, 2103. [[CrossRef](#)]
76. Aziz, S.B.; Hamsan, M.; Abdullah, R.M.; Abdulwahid, R.T.; Brza, M.; Marif, A.S.; Kadir, M.J.I. Protonic EDLC cell based on chitosan (CS): Methylcellulose (MC) solid polymer blend electrolytes. *Ionics* **2020**, *26*, 1829–1840. [[CrossRef](#)]
77. Nofal, M.M.; Aziz, S.B.; Hadi, J.M.; Abdulwahid, R.T.; Dannoun, E.M.A.; Marif, A.S.; Al-Zangana, S.; Zafar, Q.; Brza, M.A.; Kadir, M.F.Z. Synthesis of Porous Proton Ion Conducting Solid Polymer Blend Electrolytes Based on PVA: CS Polymers: Structural, Morphological and Electrochemical Properties. *Materials* **2020**, *13*, 4890. [[CrossRef](#)]
78. Shamsuri, N.A.; Zaine, S.N.A.; Mohamed Yusof, Y.; Shukur, M.F. Ion conducting methylcellulose-polyvinyl alcohol blend based electrolytes incorporated with ammonium thiocyanate for electric double layer capacitor application. *J. Appl. Polym. Sci.* **2022**, *139*, 52076. [[CrossRef](#)]
79. Aziz, S.B.; Nofal, M.M.; Abdulwahid, R.T.; Ghareeb, H.O.; Dannoun, E.M.A.; Abdullah, R.M.; Hamsan, M.H.; Kadir, M.F.Z. Plasticized Sodium-Ion Conducting PVA Based Polymer Electrolyte for Electrochemical Energy Storage—EEC Modeling, Transport Properties, and Charge-Discharge Characteristics. *Polymers* **2021**, *13*, 803. [[CrossRef](#)]
80. Hadi, J.M.; Aziz, S.B.; Brza, M.A.; Kadir, M.F.Z.; Abdulwahid, R.T.; Ali Al-Asbahi, B.; Ahmed Ali Ahmed, A. Structural and energy storage behavior of ion conducting biopolymer blend electrolytes based on methylcellulose: Dextran polymers. *Alex. Eng. J.* **2022**, *61*, 9273–9285. [[CrossRef](#)]
81. Regu, T.; Ambika, C.; Karuppasamy, K.; Rajan, H.; Vikraman, D.; Jeon, J.-H.; Kim, H.-S.; Raj, T.A.B. Proton transport and dielectric properties of high molecular weight polyvinylpyrrolidone (PVP K90) based solid polymer electrolytes for portable electrochemical devices. *J. Mater. Sci.: Mater. Electron.* **2019**, *30*, 11735–11747.

82. Ambika, C.; Karuppasamy, K.; Vikraman, D.; Lee, J.Y.; Regu, T.; Ajith Bosco Raj, T.; Prasanna, K.; Kim, H.-S. Effect of dimethyl carbonate (DMC) on the electrochemical and cycling properties of solid polymer electrolytes (PVP-MSA) and its application for proton batteries. *Solid State Ionics* **2018**, *321*, 106–114. [[CrossRef](#)]
83. Aziz, S.B.; Brevik, I.; Hamsan, M.H.; Brza, M.A.; Nofal, M.M.; Abdullah, A.M.; Rostam, S.; Al-Zangana, S.; Muzakir, S.K.; Kadir, M.F.Z. Compatible solid polymer electrolyte based on methyl cellulose for energy storage application: Structural, electrical, and electrochemical properties. *Polymers* **2020**, *12*, 2257. [[CrossRef](#)]
84. Vahini, M.; Muthuvinayagam, M. Synthesis and electrochemical studies on sodium ion conducting PVP based solid polymer electrolytes. *J. Mater. Sci. Mater. Electron.* **2019**, *30*, 5609–5619. [[CrossRef](#)]
85. Kumar, M.S.; Rao, M.C. Effect of Al<sub>2</sub>O<sub>3</sub> on structural and dielectric properties of PVP-CH<sub>3</sub>COONa based solid polymer electrolyte films for energy storage devices. *Heliyon* **2019**, *5*, e02727. [[CrossRef](#)]